Advances in Colloid and Interface Science 171–172 (2012) 1–16

Contents lists available at SciVerse ScienceDirect

Advances in Colloid and Interface Science

journal homepage: www.elsevier.com/locate/cis

Historical perspective

Shear rheology of hard-sphere, dispersed, and aggregated suspensions, and filler-matrix composites

Diego B. Genovese *

PLAPIQUI (UNS-CONICET), Camino La Carrindanga Km 7, 8000 Bahía Blanca, Argentina

ARTICLE INFO

Available online 8 January 2012

Keywords:
Shear rheology
Hard-sphere suspensions
Stabilized suspensions
Aggregated suspensions
Colloidal gels
Filler-matrix composites

ABSTRACT

This paper reviews the shear rheology of suspensions of microscopic particles. The nature of interparticle forces determines the microstructure, and hence the deformation and flow behavior of suspensions. Consequently, suspensions were classified according to the resulting microstructure: hard-spheres, stabilized, or aggregated particles. This study begins with the most simple case: flowing suspensions of inert, rigid, monomodal spherical particles (called hard-spheres), at low shear rates. Even for inert particles, we reviewed the effect of several factors that produce deviations from this ideal case, namely: shear rate, particle shape, particle size distribution, and particle deformability. Then we moved to suspensions of colloidal particles, where interparticle forces play a significant role. First we studied the case of dispersed or stabilized suspensions (colloidal dispersions), where long range repulsive forces keep particles separated, leading to a crystalline order. Second we studied the more common case of aggregated or flocculated suspensions, where net attractive forces lead to the formation of fractal clusters. Above the gelation concentration (which depends on the magnitude of the attractive forces), clusters are interconnected into a network, forming a gel. We differentiate between weak and strong aggregation, which may lead to weak or strong gels, respectively. Finally, we reviewed the case of filler/matrix composite suspensions or gels, where rigid or viscoelastic particles (fillers) are dispersed in a continuous viscoelastic material (matrix), usually a gel. For each type of suspension, predictive curves of fundamental rheological properties (viscosity, yield stress, elastic and complex moduli) vs. particle volume fraction and shear rate were obtained from theoretical or empirical models and sound experimental data, covering ranges of practical interest.

Contents

1. Introduction . . . 2
2. Hard-sphere suspensions . . . 3
   2.1. Effect of shear rate . . . 4
   2.2. Effect of particle shape . . . 5
   2.3. Effect of particle size distribution . . . 6
   2.4. Effect of particle deformability . . . 7
3. Colloidal suspensions . . . 7
   3.1. Dispersed or stabilized suspensions (dispersions) . . . 8
   3.2. Aggregated suspensions . . . 10
      3.2.1. Weakly aggregated suspensions . . . 11
      3.2.2. Strongly aggregated suspensions — colloidal gels . . . 13
4. Composite (or filled) suspensions and gels . . . 14
5. Conclusions . . . 16
Acknowledgments . . . 16
References . . . 16

* Planta Piloto de Ingeniería Química, Camino La Carrindanga Km 7, 8000 Bahía Blanca, Argentina. Tel.: +54 291 4861700; fax: +54 291 4861600.
E-mail address: dgenovese@plapiqui.edu.ar.

0001-8686/$ – see front matter © 2012 Elsevier B.V. All rights reserved.
doi:10.1016/j.cis.2011.12.005

1. Introduction

The words *dispersion* and *suspension* have often been used indiscriminately to describe a biphasic system where a solid phase is dispersed in a continuous fluid or, in other words, particles suspended in a fluid. The expression *dispersed phase* suggests that particles are kept apart from each other due to the action of either shear forces, or repulsive (or dispersive) interparticle forces. However, this is not always the case. In quiescent conditions, and when attractive forces dominate, particles tend to be aggregated or flocculated, instead of dispersed. Consequently, we will use the general term suspension, considering a dispersion to be the particular case of a dispersed (or stabilized) suspension. For the same reason, we will not refer to the particles as the dispersed phase, but the *discrete phase*. Then, we define a suspension as a biphasic system, where a continuous and a discrete phase coexist in a given volume. The particles are the elemental units constituting the discrete phase. Even in the case of particles forming a continuous network, we may refer to it as a discrete phase because its basic units are discrete particles.

In this work, we will study the rheology of *microscopic suspensions*, with particles ranging in the order of 10^{-3} to 10^{2} μm, suspended in a solvent represented as a continuum fluid. Why this size range? Suspensions with particles smaller than the order of 10^{-3} μm are called sub-nanometer-size suspensions. In this case, when the particle size has atomic dimensions, the system consists of a molecular or ionic dispersion, although strictly speaking it is a one-phase (not a biphasic) system [1], and the continuum approximation of the solvent becomes questionable [2]. On the other extreme, it is very difficult (often not possible) to obtain fundamental rheological properties (independent of sample's size and shape, and measuring system) of suspensions with particles $>10^{2}$ μm.

First, we'll study suspensions where the continuous phase is a viscous fluid (or liquid), and the discrete phase is either solid (particles), or liquid (droplets). The latter liquid–liquid suspensions are called emulsions. In the particular case of hardly deformable microscopic droplets, they behave very much like solid particles. As a result, rheological models given for solid–liquid suspensions are applicable to this type of emulsions [3]; otherwise the effect of particle deformability shall be considered, as explained in Section 2.4. The type of dominant particle interactions determines the microstructure of the discrete phase, and hence the flow behavior of the suspension. According to this, suspensions may be classified as:

1. *Hard-sphere suspensions*: no interparticle forces other than infinite repulsion at contact. These rigid, inert, spherical particles are called hard-spheres (Fig. 1a–b).
2. *Dispersed or stabilized suspensions (dispersions)*: net repulsive forces keep particles separated (Fig. 1c–d).
3. *Aggregated suspensions*: net attractive forces produce particle aggregation (Fig. 1e). Above the gelation concentration, aggregates interconnect into a network, forming a gel (Fig. 1f). They may be classified as:
   a. *Weakly aggregated suspensions:* aggregation is weak and reversible (flocculation). Gels are weak.
   b. *Strongly aggregated suspensions — colloidal gels*: aggregation is strong and irreversible (coagulation). It may lead to strong (real) gels at low particle concentrations.

Finally, we will study *filler–matrix composite* (or *filled*) *suspensions or gels*, where the continuous phase is a viscoelastic material (usually a gel), called matrix, and the discrete phase is constituted by viscoelastic particles or droplets, called fillers (Fig. 1g–h).

Three kinds of forces coexist to various degrees in flowing suspensions: hydrodynamic, Brownian, and colloidal forces [2]. Hydrodynamic (or viscous) forces exist in all flowing suspensions and arise from the relative motion of particles to the surrounding fluid. The Brownian force is the ever-present thermal randomizing force.

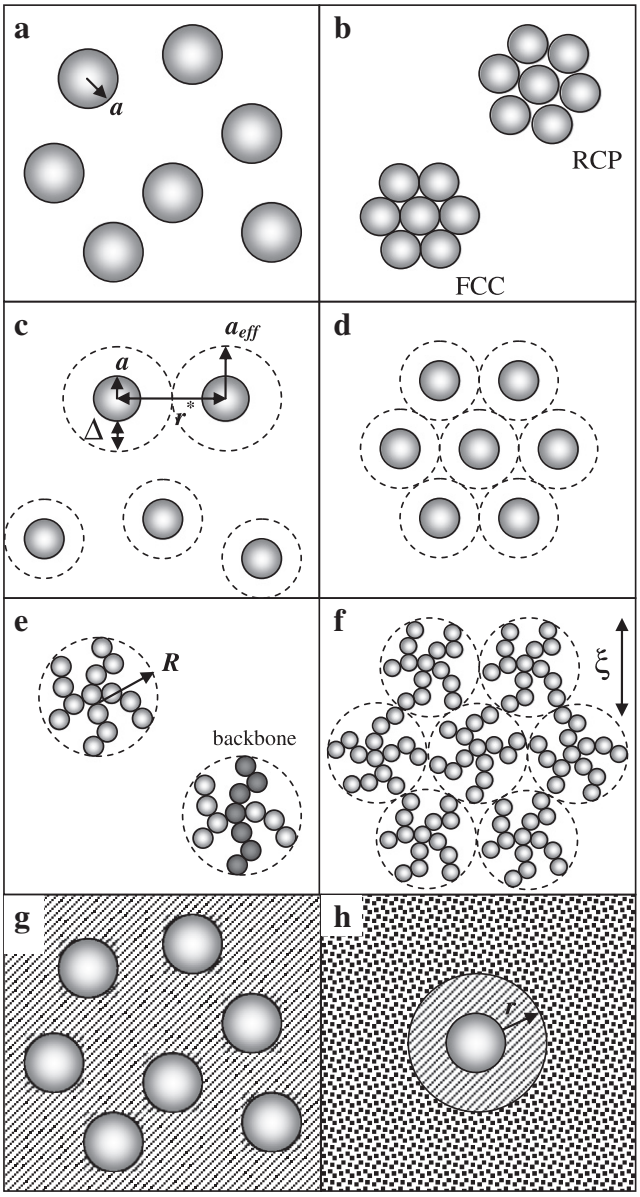

Fig. 1. Schematic representation of a) isolated hard-spheres, b) caged and packed monodisperse spheres at random close packing (RCP), and face centered cubic array (FCC), c) isolated repelling particles (dashed line represents the range of the repulsive potential), d) caged repelling particles, e) isolated fractal clusters of aggregated particles (dashed line represents the smallest enclosing sphere), f) network of fractal clusters, g) filler (spheres)–matrix (dashed background) composite, f) Van der Poel–Smith model (particulate background represents the homogeneous composite).

Colloidal forces are potential forces and are elastic in nature [4,5]. The relative magnitude of these forces and, therefore, the bulk rheology depend on the particle size (d). Brownian motion and interparticle forces quickly equilibrate for sub-nanometer-size suspensions, while hydrodynamic forces dominate for particles larger than ~10 μm. For particles in the intermediate range (10^{-3} μm$<d<10^{1}$ μm) the flow behavior is determined by a combination of hydrodynamic forces, Brownian motion, and interparticle forces [5,6].

The viscosity of flowing suspensions depends on the shear rate, and the characteristics of the continuous phase and the discrete phase. In general, the viscosity of the suspension (η) is directly proportional to the viscosity of the continuous phase, or liquid's viscosity (η_L), which might be Newtonian or non-Newtonian. Then, most

rheological models are expressed in terms of the relative viscosity of the suspension (η_r), defined as:

$$\eta_r = \eta/\eta_L. \quad (1)$$

2. Hard-sphere suspensions

We'll begin this study from the simplest case: suspensions of hard-spheres (Fig. 1a), sometimes referred to as neutral stability systems [7]. Hard spheres are considered to be rigid spherical particles, with no interparticle forces other than infinite repulsion at contact. In other words, there are no attractions or long range repulsion between the particles, but only excluded volume interaction potential. This could be the case of either non-colloidal particles (i.e. glass beds in Aroclor), or colloidal particles where repulsive and attractive forces are screened (i.e. crosslinked polystyrene lattices in a variety of solvents, silica spheres with grafted octadecyl chains dispersed in cyclohexane) [7,8]. In the flow behavior of hard sphere suspensions, interparticle forces are negligible in front of hydrodynamic forces and Brownian diffusion. Metzner [9] also suggested that when the viscosity of the continuous phase is very high (more than about 100 Pa.s) particle–particle interactions could be negligibly small compared to viscous forces.

Then, the viscosity of hard-sphere suspensions is affected by viscous forces, Brownian motion, and the excluded volume of the particles [10]. Brownian motion is ever-present and arises from thermal randomizing forces that ensure that the particles undergo constant translational and rotational movements. However, Brownian motion is only noticeable for particles smaller than roughly 1 μm [4]. Consequently, hard-spheres have been classified as Brownian or non-Brownian, depending on their size [5]. The flow of suspensions of non-Brownian hard-spheres is totally dominated by hydrodynamic forces, while Brownian hard-spheres interact through both hydrodynamic and Brownian diffusion forces. Brownian hard-spheres are non-aggregating colloidal particles.

The hydrodynamic disturbance of the flow field induced by solid particles in liquid media leads to an increase in the energy dissipation and an increase in viscosity [4]. At low particle concentrations (in the dilute regime), the relative viscosity of hard-sphere suspensions was first described by the oft-quoted theoretical equation of Einstein [11,12]:

$$\eta_r = 1 + [\eta]\phi \quad (2)$$

where ϕ and $[\eta]$ are the volume fraction and the intrinsic viscosity of the particles, respectively. Theoretically, $[\eta]$ depends on particle shape, being 2.5 for rigid spheres [3], assuming the no-slip condition between the liquid and the particle surface, which is normally well fulfilled for isolated particles.

At higher concentrations, particle crowding produce hydrodynamic interactions (as well as increasing probability of collision) between particles, resulting in significant positive deviations from Eq. (2) (Fig. 2). Many models have been proposed to describe the concentration dependence of the relative viscosity of concentrated suspensions. One of the most useful expressions is the semiempirical equation of Krieger and Dougherty [13] for monodisperse suspensions:

$$\eta_r = \left(1 - \frac{\phi}{\phi_m}\right)^{-[\eta]\,\phi_m} \quad (3)$$

where ϕ_m is the maximum packing fraction of particles. As particle concentration approaches the level corresponding to a dense packing of particles (ϕ_m), there is no longer sufficient fluid to lubricate the relative motion of particles, and the viscosity rises to infinity [9] (Fig. 2). At this point the suspension shows a shear yield stress [4]. Although the theoretical ϕ_m value of monodisperse spheres is 0.74 (in a face-centered cubic, FCC array), experimental observations have shown that loose random packing is close to 0.60, and that dense random packing (or random close packing, RCP) is close to 0.64 [5,14,15] (Fig. 1b). Suspensions become solids at rest beyond random close packing, but a finite stress can induce flow and produce significant order [10].

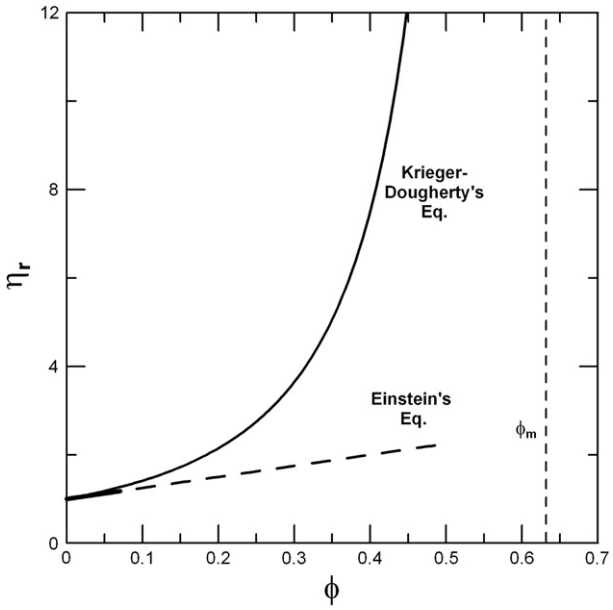

Fig. 2. Relative viscosity vs. particle volume fraction predicted by Einstein's equation for dilute hard-sphere suspensions (Eq. (2) with $[\eta] = 2.5$), and Krieger–Dougherty's equation for concentrated hard-sphere suspensions (Eq. (4) with $\phi_m = 0.63$).

It should be noted that before the volume fraction of particles reaches ϕ_m, suspensions of Brownian hard-spheres at rest present a first order thermodynamic phase transition, the onset of which is the appearance of crystals (clusters of particles) at $\phi_F = 0.494$. This point of disordered fluid to crystal transition was called the freezing concentration. Crystal and liquid phases coexist up to $\phi_M = 0.545$, called the melting concentration, where a transition to fully crystalline state (face-centered cubic order) occurs. Further increase in concentration leads to the formation of a colloidal glassy (non-ergodic) state at $\phi_G = 0.58$, called the glassy concentration, where caging stops all long-range particle motion and the dynamics becomes arrested [2,14,16,17]. If particles are not in touch due to repulsive forces (as described in Section 3.1), the system is called repulsive hard-sphere glass, or just repulsive glass. If short-ranged attractions are introduced in this state, the repulsive glass melts, and on further increase of the attraction strength it would freeze again into an amorphous solid glass. However in this case it is the attractive bonding between the spheres which forms the glass, and these are termed attractive glasses. This repulsive glass–fluid–attractive glass transition has been called the reentrant glass transition [18–21].

The mode-coupling theory (MCT) has been successfully applied to predict these two glass transitions, and has shown that the formation of repulsive and attractive glasses is caused by dynamical arrest due to caging and bonding, respectively. These two arrest mechanisms seem to dominate also the mechanical response to deformations. The framework of MCT can be extended to address the relationship between stress and strain rate in a system undergoing shear; this includes a way to relate the yield stress or shear modulus of an arrested phase to its static structure factor as determined in an unstrained state by static light scattering data [2,19–25]. MCT has also been extended to volume fractions below the glass transition to predict gel formation. However, this approach is still open to debate because gel structure has been shown to be heterogeneous, and

heterogeneous structures over a wide range of length scales are not explicitly included in MCT [26].

The exact volume fraction at which low shear viscosity diverges to infinity is still a matter of debate. Different values have been reported in the literature: 0.58 (glass transition), 0.60 (loose random packing), and 0.63 (close to dense random packing) [14], although the first one ($\phi_m = 0.58$) is commonly accepted for repulsive glasses at low shear stresses.

Practical experience shows that the product $[\eta].\phi_m$ in Eq. (3) is often around 2 for a variety of situations [3,8,14]. Then, Krieger–Dougherty's equation is usually simplified to:

$$\eta_r = \left(1 - \frac{\phi}{\phi_m}\right)^{-2}. \tag{4}$$

Hydrodynamic forces, and consequently the relative viscosity (and ϕ_m) of hard-sphere suspensions, are also affected by shear rate, particle shape, particle size distribution, and particle deformability [3,4,9,27]. When the suspended particles can no longer be considered monodisperse hard-spheres (as in most real systems), their maximum packing fraction deviates from the theoretical value ϕ_m. In this case, an effective maximum packing fraction, $\phi_{m,eff}$, is defined as the maximum packing fraction of particles that are not hard-spheres. Replacing ϕ_m, with $\phi_{m,eff}$ in Eq. (4) gives:

$$\eta_r = \left(1 - \frac{\phi}{\phi_{meff}}\right)^{-2}. \tag{5}$$

Eq. (5) is a general expression to calculate the relative viscosity of suspensions of particles that are not monodisperse hard-spheres. The value of $\phi_{m,eff}$ has to be determined for each particular system, as will be described in the next sections. It can be empirically obtained by extrapolation of $\eta_r^{-1/2}$ vs. ϕ data, from the intercept of the abscissa.

Computer simulations have made significant contributions to the theoretical development on the rheology of concentrated Brownian hard-sphere suspensions. The major difficulty has been to account for the many-body thermodynamic and hydrodynamic interactions. The most widely used method for simulating suspension flow at low Reynolds number (Re<<1 for the particle motion) has been Stokesian dynamics, developed by Brady and co-workers (see for example the review article of Brady [28] and references therein). This method properly accounts for the solvent-induced multibody hydrodynamic forces, Brownian forces, and lubrication forces [2,4,29,30]. A special subset of the Stokesian dynamics method are the Brownian dynamics simulations, where all hydrodynamic interactions are ignored [28].

2.1. Effect of shear rate

At low particle concentrations, the viscosity of hard-sphere suspensions (Eq.(2)) is independent of shear rate ($\dot{\gamma}$). At higher concentrations, the viscosity exhibits a typical 3-stage dependence with shear rate: 1) at low shear rates they show Newtonian behavior, with a constant zero-shear viscosity (η_0); 2) at intermediate shear rates the viscosity decreases following a shear-thinning behavior; and 3) at high shear rates the viscosity attains a limiting and constant value, the infinite-shear viscosity (η_∞). The decrease in viscosity at increasing shear rates is either due to alignment of suspended particles in the direction of flow, or to the shear thinning behavior of the suspending liquid (the continuous phase) [9]. This type of behavior can be correlated with the well known Cross equation [31].

As a result, for a given volume fraction of particles, the relative viscosity decreases at increasing shear rates (Fig. 3). This manifests itself in Eq. (4) as an increase in the value of the maximum packing fraction, from $\phi_{m0} \approx 0.63$ at the zero-shear limit, to $\phi_{m\infty} \approx 0.71$ at the infinite-shear limit, for monodisperse spheres [3,8,10]. Since relative

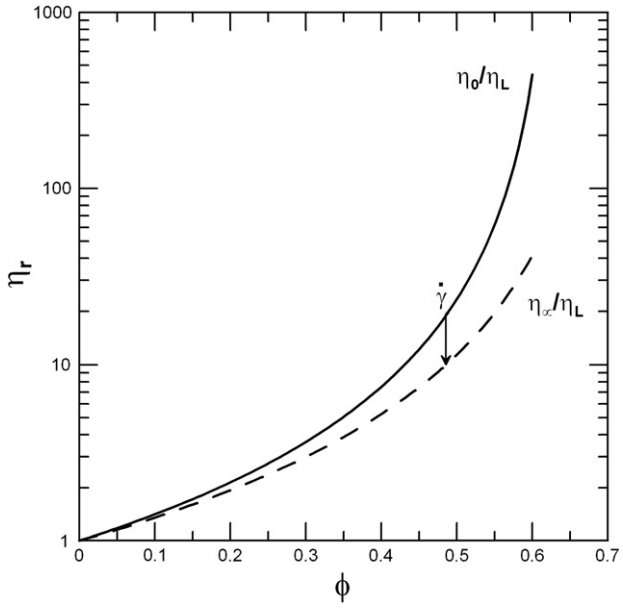

Fig. 3. Zero shear and infinite shear relative viscosities vs. particle volume fraction of hard-sphere suspensions predicted by Eq. (4) with $\phi_{m0} \approx 0.63$ and $\phi_{m\infty} \approx 0.70$, respectively. Arrow indicates the effect of increasing shear rate for a given particle volume fraction.

viscosity of hard-sphere suspensions is shear rate dependent (it might be called *apparent* relative viscosity), care must be taken to define or identify its corresponding shear rate (or shear stress). Much of the experimental data published have been obtained at the low shear limit. The zero-shear viscosity is also much better defined principally and experimentally than an infinite-shear viscosity, as practically it is very difficult to define at which shear rate one observes such a high shear limit.

It is important to note that shear thickening has been observed in highly concentrated suspensions ($\phi > 0.4$–0.5) at very high shear rates [3,4]. In these specific cases, if one continues to increase the shear rate after the viscosity has leveled off at η_∞, above a critical shear rate ($\dot{\gamma}_c$) the viscosity begins to increase again [32]. The onset of shear thickening can occur gradually or abruptly [4], but the increase in viscosity has rarely been seen to exist over more than one decade of shear rate [32]. Shear thickening is generally caused by shear-induced changes in the microstructure of the suspension, and is mostly reversible [3,4]. If the shear rate/shear stress is high enough, the particle ordering is disrupted; clumps of particles are formed, with the resulting increase in viscosity (the increase of viscosity due to particle aggregation will be explained in Section 3.2). This increase becomes more and more abrupt as the particle concentration is increased [3].

Barnes [32] reviewed the shear thickening behavior of suspensions of non-aggregating solid particles, and concluded that it is mainly affected by particle volume fraction, size and size distribution, shape, and inter-particle interactions. First, he showed that $\dot{\gamma}_c$ decreased at increasing values of ϕ, and that $\dot{\gamma}_c$ increased rapidly at $\phi << 0.5$. This means that it is experimentally more and more difficult to attain $\dot{\gamma}_c$ as ϕ decreases below 50%; but not finding $\dot{\gamma}_c$ does not mean it does not exist. Then he concluded that shear thickening should take place in all dispersions, if measured in the appropriate shear rate range. On the other hand, he showed that $\dot{\gamma}_c$ tends to zero for monodisperse suspensions at $\phi \approx 0.6$, which represents the maximum packing fraction (ϕ_m). He pointed out that ϕ_m always scales the effect of particle volume fraction, thus an increase in ϕ_m would reduce the degree of shear thickening (increase $\dot{\gamma}_c$) in a suspension and vice versa. Second, he showed that $\dot{\gamma}_c$decreases at increasing particle sizes (range 0.01–100 μm), with an inverse quadratic dependence. Third, he showed that $\dot{\gamma}_c$increases with the

number of particle classes or the width of a continuous particle size distribution, which was attributed to an increase in ϕ_m (the increase of ϕ_m with polydispersity will be explained in Section 2.3). Fourth, he showed that shear thickening increases with more anisotropic particles, which could be an effect of shape alone, or to a decrease in ϕ_m (the decrease in ϕ_m with particle aspect ratio will be explained in Section 2.2). Finally, he pointed out that shear thickening is expected for deflocculated suspensions, that is when there is no overall attraction between the particles, which is the case of particles that are either neutral (hard-spheres, as in this section) or repel one another (stabilized or dispersed, as in Section 3.1).

In the case of Brownian hard-spheres, viscous forces perturb the microstructure against the restoring effect of Brownian motion [10]. In the low shear rate regime, Brownian diffusion predominates over hydrodynamic interactions, and the suspension shows a high viscosity (η_0) due to the random arrangement of particles (Fig. 4). Inversely, in the high shear rate regime hydrodynamic forces predominate over Brownian diffusion, and the layers of particles can move freely past each other giving a low viscosity (η_∞) [7]. Both η_0 and η_∞ increase monotonically with ϕ, with shear thinning only detectable for $\phi > 0.25$–0.30, and only substantial for $\phi > 0.5$ [10]. This rheological behavior was originally described by a simple model developed by Krieger and Dougherty [13], where the apparent viscosity depends on η_0, η_∞, and the shear stress [10,33–35]. The later Cross equation is analogous to this model, but in terms of the shear rate [31]. However, the Brownian and hydrodynamic effects can be properly scaled by plotting the viscosity of the suspension as a function of the dimensionless Peclet number, instead of the shear rate or the shear stress [3]. The Peclet number is defined as the ratio of the hydrodynamic to the thermal force: $Pe = 6\pi \cdot a^3 \eta_L \dot{\gamma} / k_B T$, where $\boldsymbol{a}$ is the radius of a spherical particle (Fig. 1a), $\boldsymbol{k_B}$ is Boltzmann's constant, and $\boldsymbol{T}$ is the absolute temperature. It can also be written as $Pe = a^2 \dot{\gamma} / D_0$, where $D_0 = k_B T / 6\pi \cdot a \cdot \eta_L$ is the diffusion coefficient of an isolated sphere [33]. The value of $\boldsymbol{Pe}$ gauges the ability of flow to displace the structure from equilibrium [8,10]. Consequently, the relative viscosity of Brownian hard-sphere suspensions can be properly described by a modified Krieger Dougherty model in terms of the Peclet number [34,35]:

$$\eta_r = \eta_{r\infty} + \frac{\eta_{r0} - \eta_{r\infty}}{1 + (Pe/Pe_c)^n} \tag{6}$$

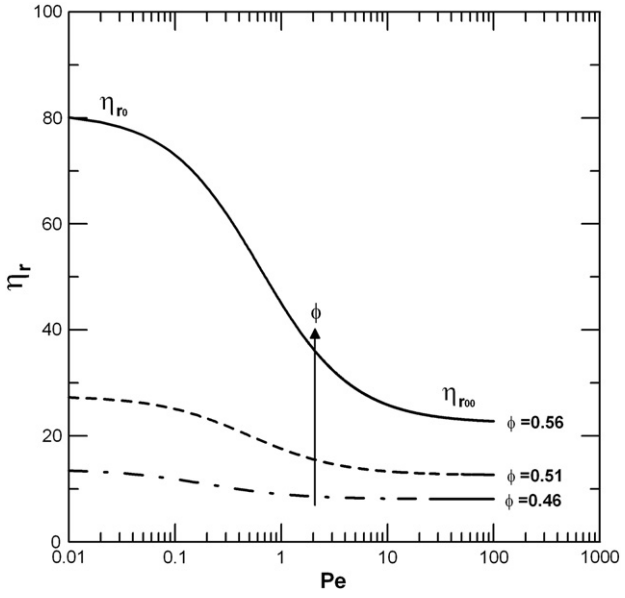

Fig. 4. Relative viscosity vs. Peclet number at different volume fractions, predicted by Eq. (6), with fitting parameters from Table 1.

where n = 1 for monodisperse suspensions, and the fitting parameter $\boldsymbol{Pe_c}$ is a characteristic Peclet number, which depends on the volume fraction of particles. Expressions for $\eta_{r0}(\phi)$ and $\eta_{r\infty}(\phi)$ may be obtained by replacing $\phi_{m0} \approx 0.63$ and $\phi_{m\infty} \approx 0.71$ into Eq. (4), respectively. Iwashita and Yamamoto [35] simulated the rheological behavior of Brownian hard-sphere suspensions using a direct numerical method, at different volume fractions and within an approximate $\boldsymbol{Pe}$ range between 10^{-2} and 10^2, and found that viscosities remained nearly constant for $\phi < 0.4$, and showed the described non-Newtonian behavior for $\phi > 0.4$. They fitted data obtained for $\phi = 0.46$, 0.51, and 0.56 using Eq. (5) with n = 1, and obtained the corresponding values of $\boldsymbol{Pe_c}$ (Table 1). Values of η_{r0} and $\eta_{r\infty}$ were obtained for each of these volume fractions (Table 1), and used in combination with $\boldsymbol{Pe_c}$ values in Eq. (6) to generate predictive curves of relative viscosity as a function of Peclet number, at different volume fractions of particles (Fig. 4).

Shear thickening has also been found in highly concentrated Brownian hard-sphere suspensions at high Peclet numbers (above the $\eta_{r\infty}$ region), which was attributed to an increase in the hydrodynamic contribution to the stress because of shear induced dynamic cluster. The onset of thickening is only due to the cluster formation when hydrodynamic forces overcome Brownian contribution [4,8,28,29].

2.2. Effect of particle shape

When the particles are non-spherical there is an extra energy dissipation and consequently an increase in the viscosity. In dilute suspensions this increase is reflected by the intrinsic viscosity in Einstein equation (Eq. (2)). For prolate ellipsoids (~ fiber or rod shape) and oblate ellipsoids (~ disk shape), Simha [36] derived Eqs. (7) and (8), respectively:

$$[\eta] = \frac{14}{15} + \frac{q^2}{15(\log 2 \cdot q - 3/2)} + \frac{q^2}{5(\log 2 \cdot q - 1/2)} \tag{7}$$

$$[\eta] = \frac{16}{15} \frac{q}{\tan^{-1} q} \tag{8}$$

where $\boldsymbol{q}$ is the axial ratio of the ellipsoid (long radius/short radius). Simpler formulas have been derived by Barnes [3] as $[\eta] = 0.07 * \boldsymbol{q}^{5/3}$ for rod-like particles, and $[\eta] = 0.3 * \boldsymbol{q}$ for disc-like particles.

The effect of particle shape on concentrated suspensions was studied by Kitano et al. [37], who proposed an equation for suspensions of non-spherical particles, equivalent to Eq. (5). They found that the effective maximum packing fraction decreased as the aspect ratio (L/D) of the suspended particles increased; for example when L/D = 1 (spheres) $\phi_{m,eff} = \phi_m$, when 6 < L/D < 8 (rough crystals) $\phi_{m,eff} = 0.44$, and when L/D = 18, 23, 27 (fibers) $\phi_{m,eff} = 0.32$, 0.26, 0.18 respectively [9,31]. Fig. 5 shows how the relative viscosity increases at increasing aspect ratios (non-sphericity) of the particles, for a given volume fraction. In general, particle non-sphericity produces an increase in the intrinsic viscosity and a decrease in the maximum packing fraction, but their product remains ≈2 (see Eqs. (4) and (5)) [3]. By definition these systems are no longer hard-sphere suspensions, but suspensions of anisometric particles.

Table 1
Characteristic Peclet number, zero-shear and infinite-shear relative viscosities at three different volume fractions of particles. Values obtained as described in Section 2.1.

ϕ	Pe_c	η_{r0}	$\eta_{r\infty}$
0.46	0.20	13.73	8.07
0.51	0.50	27.56	12.60
0.56	0.63	81.00	22.40

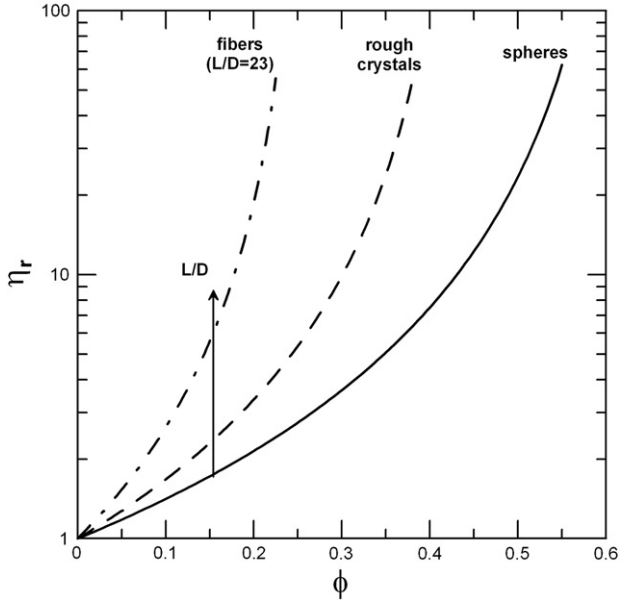

Fig. 5. Relative viscosity vs. particle volume fraction of suspensions with particles of different shapes, predicted by Eq. (5) for spheres ($\phi_{m,eff}=0.63$), rough crystals ($\phi_{m,eff}=0.44$), and fibers with aspect ratio L/D = 23 ($\phi_{m,eff}=0.26$). Arrow indicates the effect of increasing aspect ratio (non-sphericity) for a given particle volume fraction.

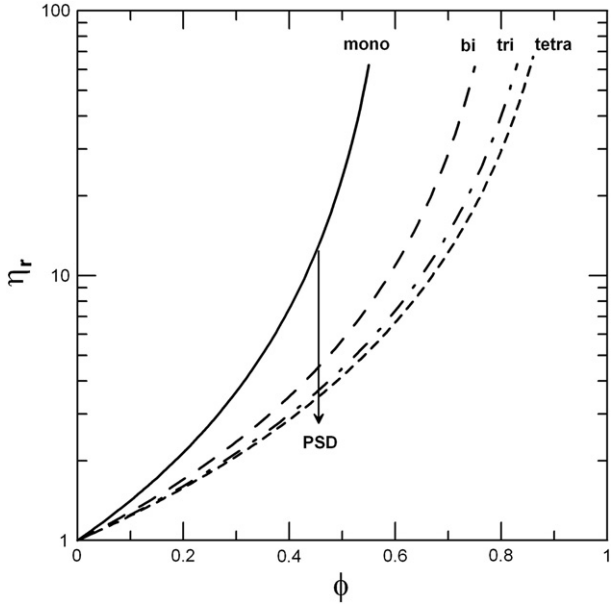

Fig. 6. Relative viscosity vs. particle volume fraction of suspensions of polydispersed spheres, predicted by Eq. (5) for monomodal ($\phi_{m,eff}=0.63$), bimodal ($\phi_{m,eff}=0.86$), trimodal ($\phi_{m,eff}=0.95$), and tetramodal ($\phi_{m,eff}=0.98$) suspensions, with infinite size ratios. Arrow indicates the effect of increasing particle size distribution for a given particle volume fraction.

2.3. Effect of particle size distribution

Eqs. (3) and (4) are valid for monomodal spherical particles, or monodispersed spheres. For suspensions of multimodal or polydispersed spherical particles, the maximum packing fraction is higher since small particles may occupy the space between the larger particles, and extraordinarily high solid concentrations can be achieved [9]. Under flow conditions, the small particles act as a lubricant for the flow of the larger particles, thereby reducing the overall viscosity [15]. This has little effect in the viscosity of dilute suspensions ($\phi<0.2$), but at high concentration levels the effects are of enormous magnitude [9]. Then, the effect of increasing the particle size distribution (PSD) is to increase the effective maximum packing fraction, $\phi_{m,eff}$, and to decrease the relative viscosity, η_r (Eq.(5)). However, $\phi_{m,eff}$ not only depends on the number of discrete size bands (mono-, bi-, tri-, tetra-modal, etc.), but also on the size ratio, defined as the ratio of the large particle diameter to that of the smaller ones in the next particle class, $\lambda = d_L/d_S$. For a given PSD, $\phi_{m,eff}$ increases with λ, and reaches a maximum value at infinite diameter ratio. Based on the works of Funk and Dinger [38], and Servais et al. [15], the following expression was derived for the maximum packing fraction of a PSD with n size bands, at infinite size ratio ($\lambda \to \infty$):

$$\phi_{meff} = \phi_{mn} = \phi_{m1}\left(n - \sum_{i=1}^{n-1}\phi_{mi}\right) \tag{9}$$

where ϕ_{m1} is the maximum packing fraction of a monomodal size distribution ($\phi_{m1}=\phi_m$). Using a value of $\phi_{m1}=0.63$ into Eq. (9), we calculated the effective maximum packing fractions $\phi_{m2}=0.86$, $\phi_{m3}=0.95$,and $\phi_{m4}=0.98$, for bi-, tri-, and tetra-modal size distributions, respectively. Using these values as $\phi_{m,eff}$ in Eq. (5), we obtained the predictive curves of η_r vs. ϕ for bimodal, trimodal, and tetramodal suspensions with infinite size ratios (Fig. 6). It can be observed that for a given particle volume fraction, the relative viscosity decreases at increasing particle size distribution (PSD). Moving from monomodal to bimodal distributions has a significant effect on the relative viscosity, but the benefit of increasing to greater than trimodal distributions is small [9,15].

Both $\phi_{m,n}$ and λ determine another parameter of polydispersions: the blend ratio, defined as the volume fraction of a particle class i in relation to the sum of the other classes, $\upsilon_i = \phi_i/\phi_{mn}$ [15]. For example, let's assume that the bimodal suspension with infinite size ratio described before is made up by adding to a monomodal suspension of spheres ($\phi_m=0.63$), another monomodal suspension of infinitely smaller spheres. These small spheres will fit in the voids of the large spheres, increasing the total volume fraction of spheres until $\phi_{m,eff}=\phi_{m2}=0.86$. In this new bimodal suspension, the volume fraction of the large spheres is $\phi_L=0.63$, and then the volume fraction of the small spheres is $\phi_S=0.86-0.63=0.23$. Then, the blend ratio of large spheres is $\upsilon_L=0.63/0.86=0.73$, or 73% of large particles and 27% of small particles. The same procedure may be followed to calculate the blend ratios of any PSD (tri-, tetra-modal, etc.).

As explained, the infinite size ratio is an ideal situation where the effective maximum packing fraction has an optimum value, for a given PSD. In a real suspension, the size ratio has a finite value, and the effective maximum packing fraction is smaller than the optimum. A graphical–analytical method to calculate $\phi_{m,n}$ at many different size ratios, and for any number of size classes, can be consulted in the work of Servais et al. [15]. It should be noted that a real particulate system consist of a continuous distribution of particle sizes. One method to estimate the effective maximum packing fraction of this type of system is to split the continuous distribution into many discrete intervals.

Farris [39] used a different approach to predict the viscosity of multimodal suspensions. He assembled many monomodal distributions and showed that the overall resulting viscosity was the product of the relative viscosity associated with each discrete monomodal size distribution, $\eta_{ri}(\phi_i)$, assuming no interactions between the particles of different class sizes:

$$\eta_r = \prod_{i=1}^{n}\eta_{r_i}(\phi_i). \tag{10}$$

In practice, narrowing or widening the particle size distribution is an effective way to control the viscosity of a suspension. The practical applications from this are that one can: a) minimize the viscosity at a

given volume fraction of particles or, b) maximize the solid content at a given viscosity. Up to 50-fold reductions in shear viscosity due to changes in particle size distribution, while maintaining the same solid content, have been reported [15]. This facilitates pumping, mixing and transportation in the fuel, concrete, paint and food industries. For example, this is of extreme importance for the use of commercial latex dispersions.

2.4. Effect of particle deformability

According to Barnes [3], at high concentrations deformable particles can accommodate each other at rest and squeeze past each other during flow, increasing ϕ_m and reducing $[\eta]$ in Eq. (3), resulting in a lower viscosity. By definition, these particles are no longer hard-spheres because they are not rigid, but deformable or viscoelastic spheres.

Snabre and Mills [40] proposed a microrheological model to estimate the steady state shear viscosity of concentrated suspensions of viscoelastic particles. They used a Kelvin Voigt model to describe the deformation and stable orientation of a viscoelastic particle in a simple shear field. They assumed that the particles behave like if they were surrounded by a fluid with a viscosity equal to that of the suspension at a given shear rate. This is known as the self-approach, or effective medium approximation. Then, the component of the shear strain tensor representative of the particle deformation gradient along the direction of the flow is:

$$\varepsilon_{xx} = \eta_r \frac{\Omega^2}{\Lambda(1+\Omega^2)} \tag{11}$$

where $\Omega = \dot{\gamma}\cdot\tau$ is a dimensionless shear rate called Deborah number, τ is the characteristic relaxation time of the Kelvin Voigt element, and $\Lambda = \eta_P/\eta_L$, where η_P is an effective viscosity accounting for the overall dissipative phenomena.

Snabre and Mills [40] claimed that the orientation of deformable particles along the main strain axes induces the formation of transient anisotropic microstructures with a higher ϕ_m, leading to a decrease in viscous dissipation and suspension viscosity. For weak particle deformations:

$$\phi_{meff} = \phi_m(1+\beta\cdot\varepsilon_{xx}) \tag{12}$$

where β is a constant related to the type of flow. Replacing Eqs. (11) and (12) into Eq. (5) yields:

$$\eta_r = \left[1 - \frac{\phi/\phi_m}{1+\eta_r\cdot\frac{\beta}{\Lambda}\frac{\Omega^2}{(1+\Omega^2)}}\right]^{-2}. \tag{13}$$

It can be observed that for rigid particles (hard-spheres) $\Omega = 0$ and Eq. (13) is reduced to Eq. (4). Eq. (13) is an implicit function, $\eta_r(\phi,\eta_r)$, and has to be solved by a numerical method. Assuming typical values of $\phi_m = 4/7$, $\beta/\Lambda = 0.1$ [40], and different values of Ω (0, 0.1, l, and 10), we solved Eq. (13) to obtain η_r at different values of ϕ, and the solution points were connected by lines (Fig. 7). It can be observed that for a given volume fraction of particles, viscosity of suspensions of deformable particles are lower than that of hard-spheres, and decreases at increasing values of the Deborah number.

3. Colloidal suspensions

Colloidal suspensions may be defined as byphasic systems where the discrete phase is subdivided into elemental units (particles/droplets) that are large compared to simple molecules, but small enough so that interparticle forces are significant in governing system properties. The size of colloidal particles is typically considered to be in the range of a few nanometers to a few micrometers [5,10,41]. According to the IUPAC [42]: a) a colloidal suspension is one in which the size of the particles lies in the colloidal range; b) the term colloidal refers to a state of subdivision, implying that the molecules or polymolecular particles dispersed in a medium have at least in one direction a dimension roughly between 1 nm and 1 μm, or that in a system discontinuities are found at distances of that order; c) the size limits given above are not rigid since they will depend to some extent on the properties under consideration; and d) a fluid colloidal system composed of two or more components may be called a sol.

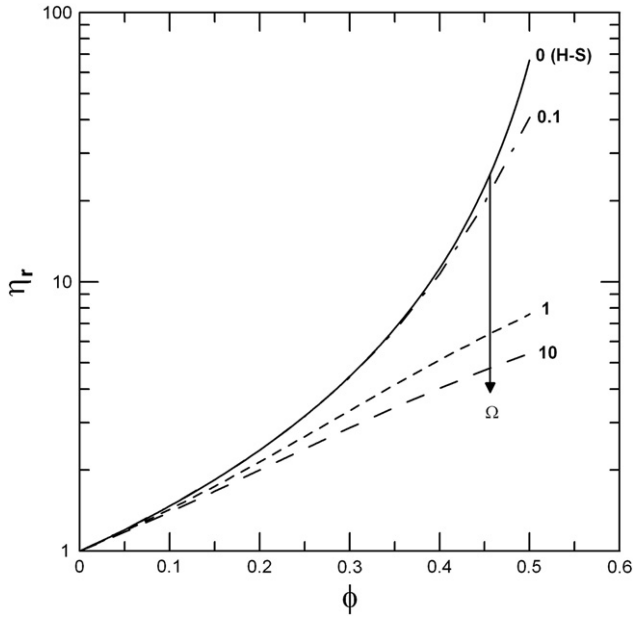

Fig. 7. Relative viscosity vs. particle volume fraction of suspensions of deformable particles, predicted by Eq. (13) with $\phi_m = 4/7$, $\beta/\Lambda = 0.1$, at different values of the Deborah number. Arrow indicates the effect of increasing particle deformability for a given particle volume fraction.

Colloidal interactions can be classified as attractive forces (including van der Waals, electrostatic attractive, hydrophobic, bridging, and depletion,) and repulsive forces (including electrostatic repulsive, steric, hydration, and structural) [4,41]. In this review, we will focus on the role of the three more relevant types of interparticle interactions, namely:

a. van der Waals attraction: the ever-present van der Waals attractive force arises from attraction between molecules that have been electronically or orientationally polarized in neighboring particles [41]. Although the intermolecular potential decays rapidly on the molecular scale, the cumulative effect is a long-range interparticle potential [10]. Its magnitude depends on the particle radius, its nature as determined by the Hamaker constant, and the interparticle distance [7].
b. Electrostatic repulsion: charged particles in an electrolyte present an arrangement of charges in the interface called the electrical double layer (EDL). As two particles approach each other, the overlapping of double layers leads to long-range, electrostatic repulsive forces. The energy–distance curve shows an approximately exponential decay. The extent of the decay depends on the thickness of the EDL, calculated as the Debye length (κ^{-1}), which in turn depends on the electrolyte concentration and valency (i.e. ionic strength). The lower the ionic strength, the higher the thickness of the EDL, the more slowly the interaction potential decays, the longer the range of interparticle interaction [7].
c. Steric repulsion: due to the presence of a polymer layer at the surface of particles, either by adsorption of chemical grafting. As two particles approach, the overlap of the polymer layers reduces the

volume available to each single chain, producing a short-range repulsive force. The lower the thickness of the polymer layer, δ, the more steeply the interparticle potential decays, the shorter the range of interparticle interaction. This is particularly the case of short adsorbed chains in good solvent conditions [4,7].

Conventionally, attractive energies are considered to be negative, and repulsive energies positive. The total or net interaction potential energy between pairs of particles as a function of the interparticle distance, $U(r)$, may be predicted by the extended DLVO theory, and is usually represented as the ratio of the interaction energy to the Brownian thermal energy, $U/k_B.T$, vs. a dimensionless particle–particle separation, $(r-2.a)/a$ (Fig. 8), being r the distance between the centers of two particles, and $r-2.a$ the distance between their surfaces. The key features of the interaction potential are the primary and secondary minima, and the primary maximum [10], as will be described in the next sections.

The balance between thermal and interparticle forces determines the equilibrium behavior. Brownian motion promotes collisions between pairs of colloidal particles, while the net interparticle force determines if two colliding particles aggregate or not. Then, colloidal suspensions at equilibrium can be either dispersed or aggregated, depending if the net particle interaction energy is repulsive or attractive, respectively. Furthermore, particle–particle interactions are crucial in determining order and phase transitions [5].

Under the action of an external driving force such as shear, hydrodynamic forces come into play and compete with thermal and interparticle forces to set the structure and determine rheological properties [43]. At very high shear rates the viscosity (η_∞) is dominated only by hydrodynamic forces [3]. Thus, the magnitude of $(\eta_0-\eta_\infty)$ reflects the importance of colloidal forces in the suspension flow behavior [44].

It should be noted that the presence of any kind of interaction, either attraction or repulsion, will result in an increase in the suspension viscosity, compared to that of hard-spheres, and in some cases, a yield stress could be observed. These phenomena are determined by the magnitude of the overall interactions and the resulting suspension microstructure, as we will see in the next sections.

3.1. Dispersed or stabilized suspensions (dispersions)

According to the IUPAC [42], colloidally stable means that the particles do not aggregate at a significant rate. In stable colloidal dispersions (Fig. 1c–d) repulsive forces dominate and keep neighboring particles away from each other, leading to crystalline order liquid-like structures, or even quasi-crystal structures at high enough particle concentrations [45,46]. For flow to occur particles must be forced to move against the force fields of the other particles, demanding an extra energy [44]. The predictive models for the viscosity of colloidal dispersions are divided into two categories based on their scaling technique. One is the separation of contribution method, in which the contributions from individual factors are separated from each other. The other is the effective volume fraction method, in which all the contributions from different factors are lumped into one factor, either the effective volume fraction (ϕ_{eff}) or the effective maximum packing fraction ($\phi_{m,eff}$) [5,47].

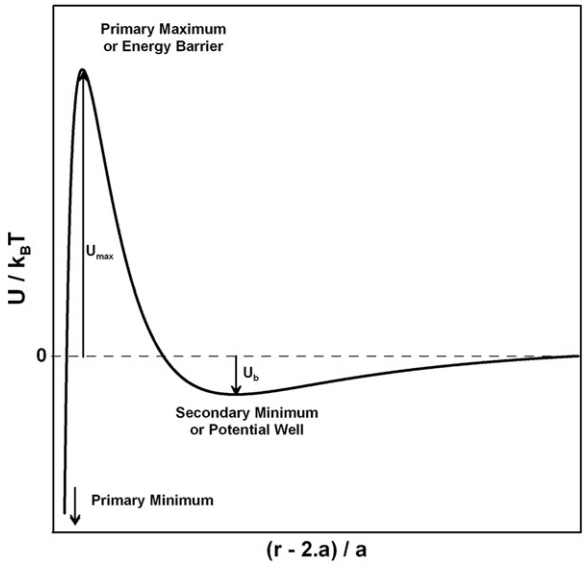

Fig. 8. Net interaction potential/Brownian thermal energy ratio vs. surface–surface interparticle distance/particle radius ratio.

In the separation of contribution method, the relative viscosity of dispersed suspensions has been modeled as the sum of a "hard-sphere" contribution (η_r^{hs}) and a "colloidal force" contribution (η_r^{cf}) [14,48]:

$$\eta_r = \eta_r^{hs} + \eta_r^{cf}. \tag{14}$$

The term η_r^{hs} is considered to be the relative viscosity of a hard-sphere suspension, and it can be calculated with Eq. (4). The term η_r^{cf} involves the increase in relative viscosity due to interparticle colloidal forces. It can be calculated from the difference between the experimental η_r data and the theoretical η_r^{hs} values.

In the case of electrostatically stabilized particles, the distortion of the EDL by the shear field leads to an increase in the viscosity due to increased energy dissipation. This effect was first considered by Smoluchowski and is called the primary electroviscous effect [49,50]. For dilute dispersions of spherical particles, it appears as a correction p, the primary electroviscous coefficient, to the Einstein equation (Eq. (2)), such that combined with Eq. (14) gives:

$$\eta_r^{cf} = 2.5 \cdot p \cdot \phi. \tag{15}$$

The coefficient $\boldsymbol{p}$ is a function of the potential in the slipping plane or ζ-potential (a measure of the particle surface potential), and the relative size of the particle radius (a) in respect to the thickness of the EDL (κ^{-1}). Several theoretical expressions have been derived for $\boldsymbol{p}$ [49,50]. Based on the theoretical model of Ogawa et al. [48] for concentrated dispersions (Eq. (17)), and own experimental data on dilute dispersions, Genovese et al. [27] proposed a general expression for $\boldsymbol{p}$ in terms of the maximum net repulsive potential between pairs of particles (U_{Max}), also known as the energy barrier or activation energy:

$$p = b \cdot \left(\frac{U_{Max}}{k_B T}\right) \tag{16}$$

where $\boldsymbol{b}$ is a dimensionless proportionality constant. The value of $\boldsymbol{U_{Max}}$ is obtained at the maximum of the $\boldsymbol{U}(r)$ curve (Fig. 8), and determines the stability of a colloidal dispersion. $\boldsymbol{U_{Max}}$ values of 15–25 $\boldsymbol{k_B.T}$ are normally required for long-term stability [51].

For concentrated dispersions, Ogawa et al. [48] derived the following expression based on the theory of activation processes:

$$\eta_r^{cf} = c_1 \phi \cdot \exp\left(\frac{U_{Max}}{k_B T} - \frac{c_2 d^3 \sigma_p}{\phi \cdot k_B T}\right) \tag{17}$$

where $\boldsymbol{c}_1$ and $\boldsymbol{c}_2$ are numerical constants, $\boldsymbol{d}$ is the particle diameter, and $\sigma_p$is the particle stress. For practical purposes, it has been assumed that $\boldsymbol{c}_1 = 1$ [48]. The exponent of e in Eq. (17) is the apparent activation potential barrier, or activation energy between two neighbor particles under shear. The first term of this exponent is the mean activation energy of the particles at rest. The second term is the bias potential created when the system is sheared, and it is the product of the activation volume by the particle stress. The activation volume

is inversely proportional to the number of particles per unit volume, then it is proportional to $\boldsymbol{d}^3/\phi$, being $\boldsymbol{c}_2$ the proportionality constant (theoretically π/6). The particle stress (or elastic stress) arises from the interparticle potential forces, and assuming that it is given by the viscosity corresponding to this activation energy (η^{cf}), it can be calculated as:

$$\sigma_p = \eta^{cf}\dot{\gamma} = \eta_r^{cf}\eta_L\dot{\gamma}. \tag{18}$$

Replacing Eq. (18) into Eq. (17) gives:

$$\eta_r^{cf} = c_1\phi\cdot\exp\left(\frac{U_{Max}}{k_BT} - \frac{c_2 d^3\eta_L}{\phi\cdot k_BT}\eta_r^{cf}\dot{\gamma}\right). \tag{19}$$

Eq. (19) is an implicit function, $\eta_r^{cf}(\phi,\eta_r^{cf})$, and has to be solved by a numerical method.

According to Eq. (17) (with $\boldsymbol{c}_1 = 1$), a plot of $k_BT\ln(\eta_r^{cf}/\phi)$ vs. σ_p should follow a linear decrease for each volume fraction, with y-intercept $\boldsymbol{U_{Max}}$ and slope $-\boldsymbol{c}_2.\boldsymbol{d}^3$. Ogawa et al. [48] fitted experimental data of styrene–butadiene particles (d≅100 nm) in water (25 °C) at different volume fractions (0.176, 0.234, 0.293, and 0.345), and obtained $\boldsymbol{U_{Max}}(\phi)$ values of about 1.80, 3.06, 4.94, and 6.66$\boldsymbol{k_B.T}$, respectively, and a unique value of $\boldsymbol{c}_2 = 0.136$. Using these values into Eq. (19), we solved it for different shear rates, and the solution points were connected by lines, at each volume fraction (Fig. 9). It can be observed that η_r^{cf} increases with ϕ and decreases with$\dot{\gamma}$, but this shear thinning effect is only noticeable at $\phi > 0.25$ approximately, and at high shear rates, where hydrodynamic forces become more significant than interparticle forces. The viscosity decrease in this shear thinning region is due to ordering of particles by the flow.

Following the shear thinning regime, a second Newtonian plateau develops, for which the viscosity attains an approximate constant value as a function of shear rate, and the flow induced ordering of the system continues to develop. At higher shear rates and for sufficiently high volume fractions, the viscosity undergoes a rapid increase once a critical value of the shear rate/shear stress is exceeded. This is the same behavior as the one described for hard-sphere suspensions (Section 2.1), although different mechanisms have been proposed. In electrostatically or sterically stabilized suspensions, the shear thickening is attributed to a shear induced order–disorder transition. In this mechanism, the particles arrange into sliding, ordered layers or planes formed during the shear thinning regime, which persist until the second Newtonian viscosity plateau. At a critical shear rate/shear stress, these layers begin to interact via hydrodynamic coupling (hydrodynamic instabilities). This interaction pulls particles out of the layers, leading to increased particle collisions, disorder, and a consequent increase in viscosity [2,4].

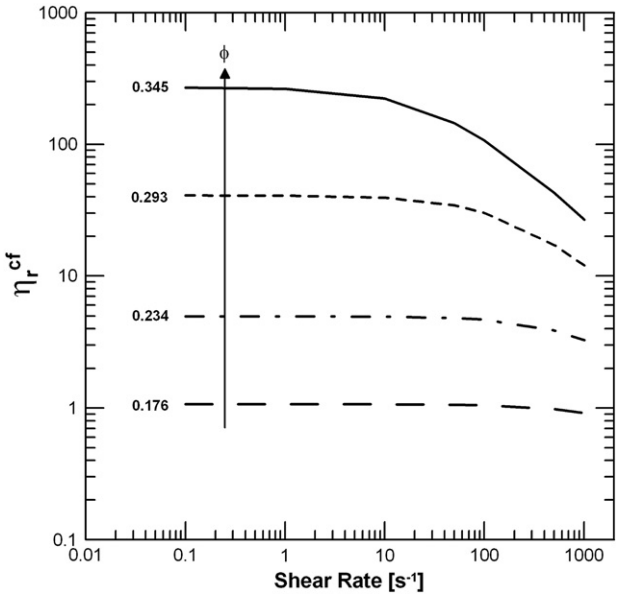

Fig. 9. Contribution of interparticle forces to relative viscosity vs. shear rate of suspensions of styrene–butadiene particles (d≅100 nm) in water, at different volume fractions, predicted by Eq. (19).

In the effective volume fraction method, it is considered that particles cannot approach each other more than a certain distance, due to the repulsive forces between them, thus increasing their apparent or effective radius from $\boldsymbol{a}$ to $\boldsymbol{a}_{eff} = r^*/2$, where r^* is the distance of closest approach [14] (Fig. 1c). In other words, particles interacting through purely repulsive potentials behave as equivalent hard spheres, with an equivalent hard sphere radius $\boldsymbol{a}_{hs} = \boldsymbol{a}_{eff}$. Consequently, the apparent volume of particles, or effective volume fraction is given as [52,53]:

$$\phi_{eff} = \phi\left(\frac{a_{eff}}{a}\right)^3 \tag{20}$$

Since $\boldsymbol{a}_{eff} > \boldsymbol{a}$, the volume occupied by the equivalent hard-spheres is bigger than the volume occupied by the real particles, then $\phi_{eff} > \phi$. In this model, particles are considered to be a core surrounded by a stabilizing or exclusion layer. Consequently, $\boldsymbol{a}$ and ϕ are usually called particle core radius, and core volume fraction, respectively. The viscosity of a colloidal dispersion can be simply obtained by replacing ϕ by ϕ_{eff} in a hard-sphere viscosity equation, like Eq. (4) [14]:

$$\eta_r = \left(1 - \frac{\phi_{eff}}{\phi_m}\right)^{-2}. \tag{21}$$

Replacing Eq. (20) into Eq. (21) gives:

$$\eta_r = \left(1 - \frac{\phi}{\phi_m}\left(\frac{a_{eff}}{a}\right)^3\right)^{-2}. \tag{22}$$

Predictive curves of η_r vs. ϕ for stabilized suspensions were obtained assuming different values of $\boldsymbol{a}_{eff}/\boldsymbol{a}$ (1, 1.1, 1.3, and 1.6) in Eq. (22) (Fig. 10). It can be observed that for a given volume fraction of particles, the relative viscosity increases as their effective particle radius increases.

When the extra excluded radius, Δ (Fig. 1c), is much smaller than the particle core radius, i.e. when $\Delta << a$, the effective particle radius, and then the effective volume fraction can be calculated from [4,5]:

$$a_{eff} = a\cdot(1 + \Delta/a) \tag{23}$$

$$\phi_{eff} = \phi\cdot(1 + \Delta/a)^3. \tag{24}$$

This approach works well for particles with a densely packed exclusion layer and a steeply decaying interaction potential, such as electrostatic repulsion at high ionic strength, and steric repulsion with short adsorbed chains in good solvent [7,14]. In these cases, $\Delta \approx \kappa^{-1}$ for electrostatically stabilized systems, and $\Delta \approx \delta$ for sterically stabilized systems.

However, when $\Delta >> a$ (such as in electrostatically stabilized systems at low ionic strength, or sterically stabilized systems with long adsorbed chains), the potential curve decays slowly and the equivalent HS radius is difficult to determine. Consequently, Eqs. (23) and (24) are no longer adequate, and experimental data deviates from Eqs. (22) and (21) respectively, due to overlapping or deformation of the exclusion layers. Particles interacting through such "soft" potentials are often called "soft spheres" [14].

In these cases where the effective particle radius (and the effective volume fraction) cannot be theoretically determined, the effective

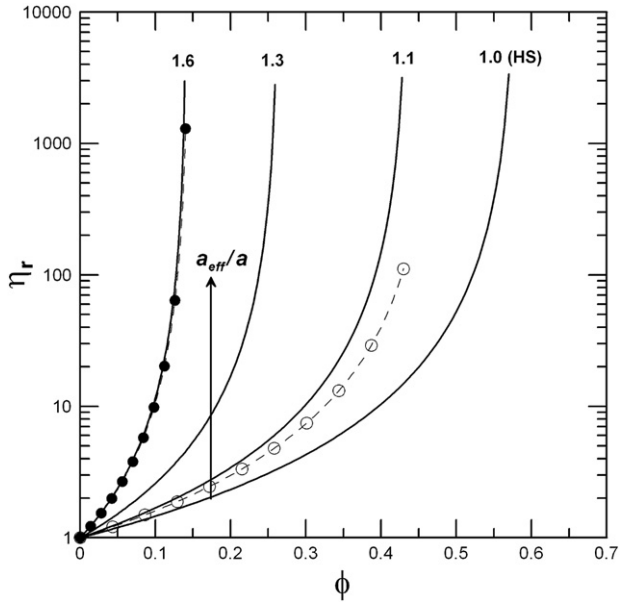

Fig. 10. Relative viscosity vs. particle volume fraction of dispersed or stabilized suspensions. Theoretical curves predicted from Eq. (22) at different values of a_{eff}/a (solid lines). Arrow indicates the effect of increasing the effective particle radius. Experimental data of electrostatically stabilized polystyrene particles in 5×10^{-4} M NaCl solution ($\phi_{m,eff}=0.144$, $a_{eff}/a=1.59$, black circles); polymethylmethacrylate particles sterically stabilized with a layer of poly-12-hydroxystearic acid ($\phi_{m,eff}=0.475$, $a_{eff}/a=1.07$, white circles).

maximum packing fraction method is preferred, and Eq. (5) is used. The value of $\phi_{m,eff}$ may be empirically obtained from a plot of $\eta_r^{-1/2}$ vs. ϕ and extrapolation to $\eta_r^{-1/2}=0$ [7], as explained in Section 2. However, in this case $\phi_{m,eff}$ does not (only) depend on particle shape, polydispersity, and deformability effects, but (also) depends on colloidal interactions and Brownian motion [47]. The system reaches the glass transition when $\phi_{eff}=\phi_G=0.58$, that is at a critical (real particle) concentration $\phi_{G,eff}$, equivalent to the effective maximum packing fraction, then $\phi_{G,eff}=\phi_{m,eff}$. The scaling relationship between $\phi_{m,eff}$ and ϕ_m is given by [5,14]:

$$\phi_{m,eff}=\phi_m\left(\frac{a}{a_{eff}}\right)^3 \tag{25}$$

As ϕ approaches $\phi_{m,eff}$, the crowding of particles strongly affects the flow behavior of the suspension, and when $\phi=\phi_{m,eff}$, an apparent yield stress develops. Since $a_{eff}>a$, the system of equivalent hard-spheres reaches the glass transition ($\phi_{G,eff}$) before the real particle concentration reaches 58% in volume, then $\phi_{m,eff}<\phi_m$.

Combining Eqs. (20) and (25) one can obtain the scaling relationship:

$$\frac{\phi_{eff}}{\phi}=\frac{\phi_m}{\phi_{m,eff}}. \tag{26}$$

It might be worth remembering that ϕ is the real volume fraction of particles, ϕ_{eff} is the apparent volume fraction of particles, $\phi_{m,eff}$ is the real volume fraction of particles when the system is packed, and ϕ_m is the volume fraction of close-packed monodisperse hard-spheres. From Eq. (26), when $\phi\to\phi_{m,eff}$, then $\phi_{eff}\to\phi_m$. Replacing Eq. (26) into Eq. (21), or Eq. (25) into Eq. (22), gives Eq. (5). This method is typically used for charged stabilized particles as well as for sterically stabilized particles.

Long range repulsive forces, such as electrostatic repulsion, lead to crystalline order at low particle concentrations [14]. For example, experimental data on electrostatically stabilized polystyrene particles ($a=34$ nm) in 5×10^{-4} M NaCl solution were satisfactorily fitted with Eq. (5) (Fig. 10), giving $\phi_{m,eff}=0.144$ [10]. This value of $\phi_{m,eff}$ was considered as the transition from a disordered fluid to either an ordered or a glassy solid ($\phi_{G,eff}$); therefore a finite stress is required to initiate flow. Above this threshold volume fraction, the dispersion behaves as a viscoelastic solid. Assuming $\phi_m=\phi_G=0.58$ in Eq. (25), it can be calculated that $a_{eff}/a\approx1.59$. Metzner [9] already have claimed that in aqueous systems, particle–particle interactions through electrostatic forces may be enormous, and even very dilute suspensions may exhibit a yield stress.

Pusey and Megen [16] studied the phase behavior of concentrated suspensions of polymethylmethacrylate (PMMA) particles ($a=305$ nm) sterically stabilized with a layer ($\Delta\approx10$–20 nm) of poly-12-hydroxystearic acid (PHSA), in a 2.66:1 decalin-carbon disulphide solvent mixture. In the effective volume fraction model (Eqs. (20) to (24)), ϕ is the volume fraction of the PMMA core, and ϕ_{eff} is the effective volume fraction that accounts for the PHSA layer. As mentioned, they found thermodynamic phase transitions at the freezing concentration $\phi=0.407$ ($\phi_{eff}=0.494$), the melting concentration $\phi=0.449$ ($\phi_{eff}=0.545$), and the glassy concentration $\phi\approx0.48$ ($\phi_{eff}\approx0.58$). From Eqs. (20) or (25) it can be calculated that $a_{eff}/a\approx1.07$. Phan et al. [54] measured the viscosity of PMMA–PHSA suspensions up to $\phi_{eff}\approx0.50$. Combining their results with experimental data reported in the literature for the same system, and fitting all the data for $0.30<\phi_{eff}<0.50$ to Eq. (21), they obtained a value of $\phi_m=0.577$, which coincides with the effective volume fraction that marks the onset to a colloidal glassy state ($\phi_G\approx0.58$). This maximum packing fraction was scaled with Eq. (25) to obtain $\phi_{m,eff}=0.475$. This value was used in Eq. (5) to represent the data of Phan et al. [54] in Fig. 10.

3.2. Aggregated suspensions

A far more widespread situation in colloidal systems is the presence of net attractive forces between particles, leading to particle aggregation [3,14]. According to the IUPAC [42]: a) an aggregate is, in general, a group of particles held together in any way and, more specifically, the structure formed by the cohesion of colloidal particles; b) when a sol is colloidally unstable (i.e. the rate of aggregation is not negligible) the formation of aggregates is called flocculation or coagulation; c) these terms are often used interchangeably, but flocculation is preferred for the formation of a loose or open network (called floc) which may or may not separate macroscopically, and coagulation is preferred for the formation of compact aggregates, leading to a macroscopic separation of a coagulum; d) the rate of aggregation is in general determined by the frequency of collisions and the probability of cohesion during collision; e) if the collisions are caused by Brownian motion, the process is called perikinetic aggregation; if by hydrodynamic motions, one may speak of orthokinetic aggregation.

The probability of cohesion is given by the interparticle potential during collision. Van der Waals interaction prevails at very small interparticle distances ($r=1$–10 nm), resulting in a minimum net interaction potential energy, called the primary minimum (Fig. 8), where the attractive forces are large enough to give permanent particle contact, or irreversible aggregation, called coagulation [3,10]. To coagulate two approaching particles, they must have enough kinetic energy (due to Brownian motion) to overcome the energy barrier ($k_B.T>U_{max}$) and fall in the primary minimum.

In many systems, the combined effect of attractive and repulsive forces produces a secondary minimum in the net interaction potential (Fig. 8). If $k_B.T<U_{max}$, the particles cannot pass the energy barrier and will fall in this local energy minimum or potential well. The depth of this potential well is a measure of the interparticle bond energy (U_b), while the position of this minimum corresponds to the most likely separation of the particles [41]. If U_b is about 10 to 20 $k_B.T$ units, the flocculation is weak and reversible [10,55,56], but no flocculation

occurs if $U_b<10\ k_B.T$ units because Brownian motion will keep the particles apart [3]. Overall, these systems may be classified as *strongly aggregated* suspensions if the interparticle bond energy is high (say $U_b>20\ k_B.T$), or *weakly aggregated* suspensions if $10\ k_B.T<U_b<20\ k_B.T$ [55].

Aggregation of colloidal particles typically leads to the formation of highly branched fractal flocs, called clusters. At low particle concentrations, clusters are not interconnected (Fig. 1 e) and the suspension remains liquid-like, or weakly elastic with no yield stress [57]. In contrast, above a critical concentration called the percolation threshold or gel point ϕ_g [4], clusters are interconnected into a network, and the system becomes solid-like (Fig. 1f), with yield stress and elastic moduli increasing with ϕ. In the former case ($\phi<\phi_g$), rheological properties are dominated by the discrete aggregates, while in the later case ($\phi>\phi_g$), mechanical properties of a continuous network are probed [57].

Gelation in aggregating colloids occurs when clusters become crowded [14]. Irreversible gelation is that in which particles gradually stick together very strongly to form permanent fractal type aggregates, which in turn eventually join together to produce large interconnected macroscopic networks. On the other hand, reversible gelation is that in which particles stick together rather weakly to form a transient network having some of the connectivity and viscoelastic properties of a weak gel-like solid [58]. In practice, the aggregation and gelation of many real systems may fall somewhere between these two situations.

Clusters can be properly treated as fractal objects because they are self-similar and remain invariant under a change of length scale [46]. The average number of elementary particles in a fractal cluster, N, is related to its average radius, R, through:

$$N\approx\left(\frac{R}{a}\right)^{f} \tag{27}$$

where $\boldsymbol{a}$ is the radius of the monosized spherical particles, and f is the fractal dimension of the cluster [3,10,45,46,55,59]. A prefix constant close to 1 can be introduced in the right-hand term of Eq. (27) depending on the definition of $\boldsymbol{R}$, which can be the hydrodynamic radius, the collision radius, the radius of gyration, or the radius of the circumscribed sphere [60]. The fractal dimension reflects the internal structure of the flocs (it is proportional to their density) and depends on the mode of aggregation [10]. Its value may range from almost 3 for the most dense, close-packed aggregates (a value of $f=3$ simply would mean a packing like in a crystal lattice), to lower values for more open structures. Typical values are $f\approx1.8$ for fast Brownian, diffusion limited cluster aggregation (DLCA), and $f\approx2.1$ for slow, reaction limited cluster aggregation (RLCA) [46,58,59,61].

Clusters are supposed to behave like spheres composed of particles in contact with trap fluid (Fig. 1e) [60]. Thus, the main effect resulting from the aggregation process is an increase in the volume of the discrete phase with respect to its nominal value, ϕ, i.e. the sum of the volumes of the constituent (elemental) particles [46]. This effect is considered by the effective volume fraction of the clusters, $\phi_c=\phi_{eff}$, defined by the smallest spheres enclosing the clusters [3,55,62,63]:

$$\phi_{eff}\approx\phi\cdot N^{\frac{3}{f}-1}\approx\phi\cdot\left(\frac{R}{a}\right)^{3-f}. \tag{28}$$

The viscosity of the aggregated suspension may be obtained by introducing the effective volume fraction of the clusters (Eq. (28)) into Eq. (21) [45,46,64]:

$$\eta_r=\left(1-\frac{\phi}{\phi_m}\left(\frac{R}{a}\right)^{3-f}\right)^{-2}. \tag{29}$$

Since $\phi_{eff}>>\phi$ ($\boldsymbol{R}>>\boldsymbol{a}$), the viscosity of the aggregated suspension (Eq. (29)) is much higher than that of the hard-sphere suspension (Eq. (4)), and the liquid–gel transition occurs at a critical value known as the gelation concentration (ϕ_g), which is then equivalent to the effective maximum packing fraction, $\phi_g=\phi_{m,eff}$, and lower than ϕ_m. The value of ϕ_g depends on the magnitude of the interaction energy at contact: the higher the attraction, the lower the critical concentration for gelation. It is worth noting that in both stabilized and aggregating colloidal suspensions, the critical concentration at which the liquid–solid transition occurs ($\phi_{m,eff}$), decreases as the magnitude of the interaction energy increases (repulsive barrier in the first case, and potential well in the other). It can also be observed from Eq. (28) (and Eq. (29)) that, unlike hard-sphere and stabilized suspensions, in aggregated suspensions the effective volume fraction (and the viscosity) depends on the size of the clusters ($\boldsymbol{R}$), via the number of elemental particles in the cluster ($\boldsymbol{N}$) [14].

3.2.1. Weakly aggregated suspensions

The shear flow breaks down the aggregates or flocs, which are restored under quiescent conditions due to the attractive force field, in addition to Brownian motion [3,10,14,55,64]. The structure recovers to a reproducible rest state in a reasonable time after shear, so the history dependence can be controlled [10,17]. At a given shear stress (σ) or shear rate ($\dot{\gamma}$), the steady state is reached when a dynamical equilibrium is established between breakdown and reformation of the aggregates [45]. At this point the aggregates reach a maximum stable (or mean equilibrium) size, $\boldsymbol{R}$. This steady state size (and the number of particles per cluster) can be predicted either from the balance between aggregate cohesion and flow related stresses, or from competition between aggregation and fragmentation dynamics [60]. It has been shown that the equilibrium value of $\boldsymbol{R}$ (and $\boldsymbol{N}$) decreases at increasing values of σ or $\dot{\gamma}$ [45]. Shearing hard enough will result in the flocs being reduced to the primary particles [3]. Consequently, above the yield stress (if $\phi>\phi_g$) the viscosity decreases from a high, zero-shear viscosity to a low, infinite-shear viscosity, through a shear thinning region at intermediate shear rates [14,45,46,59].

Different models have been proposed to describe this phenomenon, based on the fact that the maximum equilibrium size of the clusters is limited by the maximum shear stress (or torque, or momentum) that they can support before they break. Wessel and Ball [62] proposed that when the bending moment acting on the clusters due to the applied shear forces (Γ) is bigger than the binding energy between particles (Γ_c), the maximum stable cluster size ($\boldsymbol{R}$) is related to the shear stress of the solvent (σ_L), then to the shear rate ($\dot{\gamma}$) and the viscosity of the solvent (η_L), by $R\approx\sigma_L^{-1/3}\approx\left(\eta_L\dot{\gamma}\right)^{-1/3}$.

However, it has been found to be more effective to employ the already mentioned self-consistent approach, and to consider that the aggregates are surrounded by an effective medium with a viscosity equal to that of the suspension [45,46,55,60]. Then, the viscosity (or the shear stress) of the liquid solvent has been replaced by the viscosity (or the shear stress) of the suspension. Based on this criterion, Snabre and Mills [45] developed a model for fractal clusters made up of particles >1 μm, so that hydrodynamic effects dominate over Brownian motion:

$$\frac{R}{a}\approx1+\left(\frac{\sigma_c}{\sigma}\right)^{m} \tag{30}$$

where σ is the shear stress of the suspension, given by:

$$\sigma=\eta\cdot\dot{\gamma}=\eta_r\cdot\eta_L\cdot\dot{\gamma}. \tag{31}$$

The exponent m in Eq. (30) mainly depends on the structure of the aggregates, and their mechanism of deformation and breakup under the action of external stresses [45,60]. A weak bonding energy between particles (reversible flocculation) gives rise to soft clusters,

unable to transmit any elastic stresses, then deforming irreversibly the internal structure. On the other hand, in rigid clusters small elastic deformations preserve the structure of rigidly connected particles in relation with irreversible flocculation. For soft clusters $m=1/2$, and for rigid clusters $m=1/3$. In Eq. (30), σ_c is the characteristic stress for cluster break up, or characteristic cohesion stress, which depends on the strength of the particle–particle interactions. It may be related to the surface adhesive energy per unit contact area, E_a [45], or to the adhesion force, F_a, defined as the force required to separate the particles at an infinite distance from each other [60], by:

$$\sigma_c \approx E_a/a \approx F_a/a^2. \tag{32}$$

Replacing Eq. (31) into Eq. (30) gives:

$$\frac{R}{a} \approx 1 + \left(\eta_r \frac{\eta_L \dot{\gamma}}{\sigma_c}\right)^{-m} \tag{33}$$

where $(\eta_L \dot{\gamma}/\sigma_c)$ is a dimensionless shear rate. Replacing Eq. (33) into Eq. (29) gives:

$$\eta_r = \left\{1 - \frac{\phi}{\phi_m}\left[1 + \left(\eta_r \frac{\eta_L \dot{\gamma}}{\sigma_c}\right)^{-m}\right]^{3-f}\right\}^{-2}. \tag{34}$$

Eq. (34) is an implicit function, $\eta_r(\phi,\eta_r)$, and has to be solved by a numerical method. It was solved for soft clusters ($m=1/2$) and rigid clusters ($m=1/3$), assuming typical values of $\phi_m=4/7$, $f=2.0$ [45], and different values of ϕ (0.1, 0.3, and 0.5). Solution points obtained for η_r at different values of $\eta_L\dot{\gamma}/\sigma_c$ were connected by lines (Fig. 11). It can be observed that for a given volume fraction of particles, the viscosity decreases at increasing shear rates, due to the decrease in the equilibrium cluster size (and its effective volume fraction). At infinite shear rates, the clusters are reduced to the primary particles (from Eq. (33), $\boldsymbol{R} \approx \boldsymbol{a}$), and the viscosity reaches a plateau corresponding to a hard-sphere suspension (Eq. (34) is reduced to Eq. (4)).

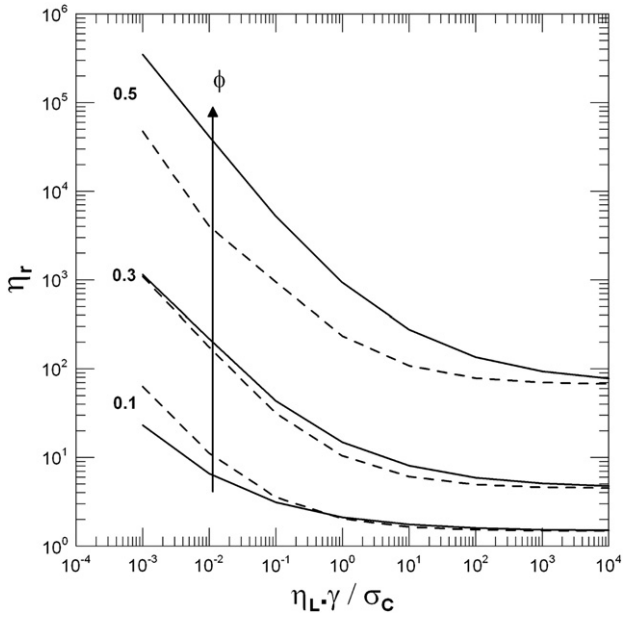

Fig. 11. Relative viscosity vs. dimensionless shear rate of weakly aggregated suspensions, predicted by Eq. (34) with $\phi_m=4/7$, and $f=2.0$, for soft clusters ($m=1/2$, dashed lines), and rigid clusters (m = 1/3, solid lines), at different particle volume fractions. Arrow indicates the effect of increasing the particle volume fraction for a given shear rate.

Potanin et al. [55] proposed a microrheological model in which the shear stress (then the viscosity) was estimated as the sum of hydrodynamic and structural contributions:

$$\eta_r = \eta_r^{hydr} + \eta_r^{struct}. \tag{35}$$

The first term (η_r^{hydr}) was attributed to the hydrodynamic cores of fractal aggregates, and was calculated from an expression analogous to Eq. (29). However, they did not follow Eq. (30), but another break up criterion, which may be consulted in the original paper. The second term (η_r^{struct}) accounts for the forces transmitted by chains of particles linking neighboring aggregates into a transient network. Soft and rigid chains were distinguished, but only the latter were considered to transmit stress through multiple connected backbones which deform as elastic contorted rods. The backbone is the fraction of the chain that is elastically active (darker particles in Fig. 1e), i.e. able to transmit elastic forces which give rise to the network stress tensor. Fig. 1.f shows the end-to-end distance of chains, or correlation length of the network, ξ. In the case of backbone chains which span the whole aggregate or connect neighboring aggregates, $\xi \approx R$. The number of particles per chain, $\boldsymbol{N_{ch}}$, is given by a relationship analogous to Eq. (27) [55,65]:

$$N_{ch} \approx \left(\frac{\xi}{a}\right)^x \tag{36}$$

where x is the chemical dimension of chains or chemical length exponent. Then, x is the dimension of the chain bearing the load. The value of x ranges between 1 (straight chains) and ~1.6 (self-avoiding random walk), while $x=1.3$ is the value expected for percolation clusters [55,57,65]. Eq. (36) was originally proposed for irreversible aggregation, and its terms will be further discussed in the next section. In the low-shear Newtonian limit the hydrodynamic interaction may be neglected, and the aggregates form a space-filling network, so that the relative viscosity is reduced to the structural contribution:

$$\eta_{r0} \approx \eta_r^{struct} \approx \frac{\alpha \cdot \tau_0 \cdot h_a}{c^2 \cdot a} \frac{\sigma_c}{\eta_L} \phi^{\frac{7+3x-2f}{3-f}} \tag{37}$$

where α is the capture efficiency of the fraction of particle collisions resulting in rigid interaggregate chains, $\tau_0 = 6.\pi.\eta_L.a^3/(k_B.T)$ is the characteristic diffusion time of an isolated particle, h_a is the equilibrium gap width between particles, σ_c as in Eq. (32) (F_a defined as the bonding force between particles), and $c = (U/k_B.T).\exp(-z.U/k_B.T)$, where z is the minimum number of bonds to be broken when a particle exchanges stable positions within the rigid chain.

As mentioned, the previous models for weakly aggregated suspensions under shear were obtained at the steady state, when the clusters reached their equilibrium size after the break-up and re-aggregation processes. These changes are not instantaneous, but require a finite time to take place. This non-equilibrium nature of the structure implies that the rheology of weakly aggregated suspensions can be affected by shear history, i.e. shear rate and time [3,10,26]. On shearing the suspension at a given shear rate, the average radius of the cluster — and consequently the viscosity — decreases (up to the equilibrium value), and on standing the cluster size — and then the viscosity — gradually recovers [3]. This time effect is called reversible thixotropy. A wide range of thixotropy models has been proposed, most of them phenomenological [26], and out of the scope of this review.

Above the percolation concentration ϕ_g, cluster growth and overcrowding result in gelation and in the appearance of an infinite spanning structure. As a result, the suspension shows a yield stress under which this network no longer flows and displays solid-like

viscoelasticity [45]. Combining Eqs. (28) and (30) the following expression may be obtained:

$$\frac{\sigma}{\sigma_c} \approx \left[\left(\frac{\phi}{\phi_{eff}} \right)^{\frac{1}{f-3}} - 1 \right]^{-\frac{1}{m}}. \tag{38}$$

The yield stress (σ_0) can be obtained by extrapolating the values of the shear stress at the zero limit of shear rate, also corresponding to an effective volume fraction ϕ_{eff} that tends to the maximum packing fraction ϕ_m. Then, for $\phi_g < \phi < \phi_m$, Eq. (38) is reduced to [45,60]:

$$\frac{\sigma_0}{\sigma_c} \approx \left(\frac{\phi}{\phi_m} \right)^{\frac{1}{m(3-f)}}. \tag{39}$$

Predictive curves of σ_0/σ_c vs. ϕ (Fig. 12) for suspensions of soft clusters ($m = 1/2$) and rigid clusters ($m = 1/2$) were obtained using values of $\phi_m = 4/7$ and $f = 2.0$ in Eq. (39).

Wessel and Ball [62] obtained the expression $\sigma_0 \approx \phi^{\frac{2}{3-f}}$, which is proportional to Eq. (39) with $m = 1/2$ (soft clusters). In the model of Potanin et al. [55], the dynamic yield stress obtained from the hydrodynamic contribution was:

$$\frac{\sigma_0^{hydr}}{\sigma_c} \approx \left(\frac{2}{5\pi} \right) \left(\frac{\phi}{\phi_m} \right)^{\frac{3}{3-f}}. \tag{40}$$

It can be noted that Eq. (40) is proportional to Eq. (39) with $m = 1/3$ (rigid clusters). On the other hand, the dynamic yield stress obtained from the structural contribution was:

$$\frac{\sigma_0^{struct}}{\sigma_c} \approx \left(\frac{2}{5\pi} \right)^{\frac{1+x}{4+x}} \left(\frac{\alpha \cdot h_a}{a} \right)^{\frac{3}{4+x}} \phi^{\frac{6}{4+x}}. \tag{41}$$

Authors [55] claimed that Eq. (41) was valid at low ϕ, while Eq. (40) at higher ϕ, and the dynamic yield stress is the maximum of both. Under small-amplitude oscillatory deformation, they obtained an expression for the high-frequency elastic modulus:

$$G'_{\infty} \approx \frac{\alpha \cdot k_0^{1/2}}{c} \sigma_c \phi^{\frac{7+2x-2f}{3-f}} \tag{42}$$

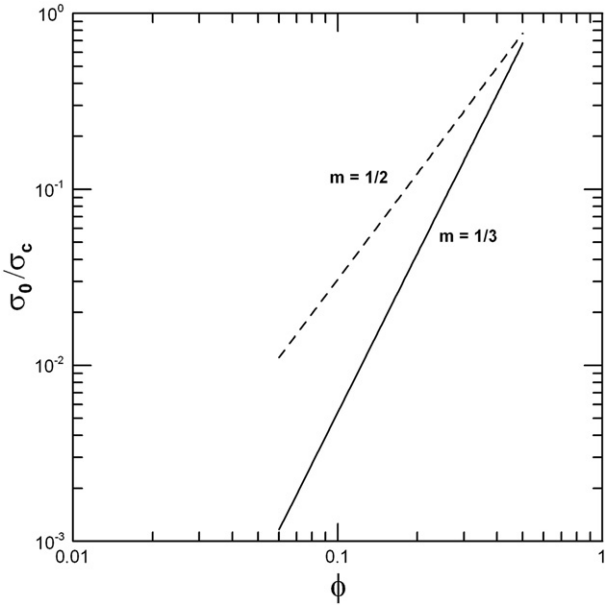

Fig. 12. Yield stress/shear stress for cluster break-up ratio vs. particle volume fraction of weakly aggregated suspensions, predicted by Eq. (39) with $\phi_m = 4/7$, and $f = 2.0$, for soft clusters ($m = 1/2$), and rigid clusters ($m = 1/3$).

where k_0 is a numerical coefficient. Chougnet et al. [60] studied the rheological behavior of cement and silica suspensions, and found good agreement between experimental data and the model of Snabre and Mills [45], both for viscosity (Eq. (34)) and yield stress (Eq. (39)).

3.2.2. Strongly aggregated suspensions — colloidal gels

When the inter-particle interaction is highly attractive, a gel structure is formed even at low particle volume fractions. A colloidal gel is a special state of flocculated systems in which a continuous network of particles is formed before settling occurs, with the resulting suspension having a very high viscosity and a finite shear modulus. According to the IUPAC, a gel is a colloidal system with a finite, usually small, yield stress [42]. Ultimately, the rheological properties of a colloidal gel depend on the response of the gel backbone, the portion of the microstructure that is active in stress transmission [61]. The load is transmitted from cluster to cluster not via all the elements inside the cluster, but only through the backbone (darker particles in Fig. 1e), in contrast to the branches attached to the backbone, which do not transmit the load [59]. The elastic backbone has been approximated as a linear chain of springs [66]. The number of springs in a floc that belongs to the backbone is given by Eq. (36), where it is equivalent to N_{ch}. Analogously, the correlation length of the network (ξ) for colloidal gels is the critical length scale for gelation, and represents the size of the closely packed fractal flocs (Fig. 1f), or blobs [66], or the size of the mesh, which is of the order of the size of the aggregates (R) that have filled the space [59]. The other term in Eq. (36), x, has been defined as the backbone fractal dimension of the flocs [66], or fractal dimension of the single bonds [59], or bond dimension, which describes the fractal geometry of the backbone structure [61]. Its value is less than the fractal dimension of the flocs (f), and larger than unity to provide a connected path [66].

Shih et al. [66] developed a scaling model to describe the viscoelastic properties of colloidal gels, well above the gelation threshold. Considering the gel network as closely packed fractal flocs, they found that the critical strain for nonlinearity and the plateau modulus depend on the strength of interactions between the flocs compared to within the flocs. When the links between flocs have a higher elasticity than those within the flocs, known as the "strong-link regime", the macroscopic elastic constant is given by [66]:

$$G' \approx \phi^{\frac{3+x}{3-f}}. \tag{43}$$

When the flocs are more rigid than the inter-floc links, which is known as the "weak-link regime" [66]:

$$G' \approx \phi^{\frac{1}{3-f}}. \tag{44}$$

Uriev and Ladyzhinsky [59] developed a model for the shear flow of low concentration colloidal gels in the solid-like and the fluid like states. Considering that the structure of these gels corresponded to a space-filling network of colloidal aggregates having a tenuous fractal structure, with rigid bonds between particles, they obtained an expression equivalent to Eq. (43):

$$G' \approx k \cdot G'_p \cdot \phi^{\frac{3+x}{3-f}} \tag{45}$$

where $\boldsymbol{G}'_p$ is the elastic modulus of the particle material, and $\boldsymbol{k} < 1$ is a dimensionless fitting coefficient accounting for the contact zone between the particles [59]. They also proposed an expression for the yield stress, based on the minimum energy required to break up the backbone connecting structure in equilibrium, i.e. the single bond energy U_b:

$$\sigma_0 \approx \frac{k \cdot U_b}{a^3} \phi^{\frac{3}{3-f}} \tag{46}$$

where $\boldsymbol{k}$ is the fitting coefficient. Finally, they developed a model for the low shear limit viscosity, which they called the "solid-like viscosity", considering that the flow was controlled by the aggregates connected into a network:

$$\eta_0 \approx k \cdot G_p^{'} \cdot \tau_b \left[\exp\left(\frac{U_b}{k_B T}\right)\right] \cdot \phi^{\frac{3+2x}{3-f}} \tag{47}$$

where τ_b is the period of the thermal oscillations of the single bond.

Pantina and Furst [61] developed a micromechanical three point bending test for the direct measurement of the particle–particle bond rigidity, κ_0, which can be used to estimate the shear elastic modulus of colloidal gels through the expression:

$$G^{'} = \frac{\kappa_0}{a}\phi^{\frac{3+x}{3-f}} \tag{48}$$

which is equivalent to Eqs. (43) and (45). Studying PMMA aggregates under various physicochemical conditions, they [61] obtained κ_0 values in the range between 0.01 and 1 N/m^2. Assuming typical values of $f = 2.0$, $x = 1.3$, and $\boldsymbol{a} = 0.5$ μm in Eq. (48), predictive curves of $\boldsymbol{G}'$ vs. ϕ at different values of κ_0 (0.01, 0.1 and 1 N/m^2) were obtained (Fig. 13).

The same authors [67] demonstrated that the yield stress of a colloidal gel can be quantitatively understood based on the critical bending moment of the underlying gel microstructure, M_c, according to:

$$\sigma_0 \approx \frac{M_c}{a^3}\left(\frac{\phi}{\phi_m}\right)^{\frac{3}{3-f}} \tag{49}$$

where $\phi_m \approx 0.64$ was considered as the point where the aggregates become close packed. Eq. (49) is equivalent to Eq. (46) with $\boldsymbol{M}_c = k.U_b$. For the same PMMA aggregates mentioned previously, Furst and Pantina [67] obtained $\boldsymbol{M}_c$ values in the range between 10^{-18} and 4×10^{-17} N.m. Using the values of $f = 2.0$, and $\boldsymbol{a} = 0.5$ μm into Eq. (49), predictive curves of σ_0 vs.ϕ at different values of $\boldsymbol{M}_c$ (10^{-18}, 10^{-17} and 10^{-16} N.m) were obtained (Fig. 14). It can be observed that for a given volume fraction of particles, both the elastic modulus (Fig. 13) and the yield stress (Fig. 14) of the gels increase at increasing interparticle bonding energy.

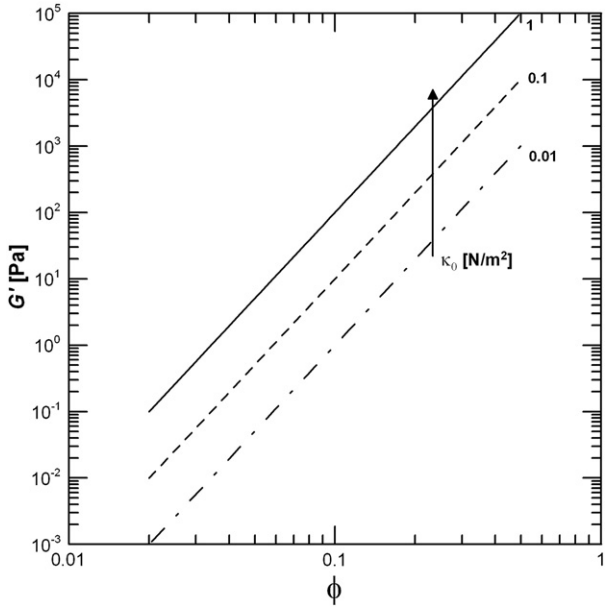

Fig. 13. Elastic modulus vs. particle volume fraction of strongly aggregated gels, predicted by Eq. (48) with $f = 2.0$, $x = 1.3$, and $\boldsymbol{a} = 0.5$ μm, at different values of particle–particle bond rigidity (κ_0). Arrow indicates the effect of increasing κ_0 for a given particle volume fraction.

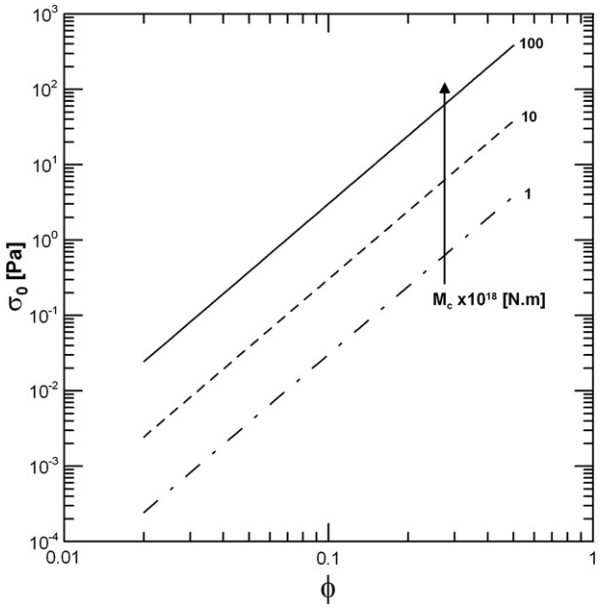

Fig. 14. Yield stress vs. particle volume fraction of strongly aggregated gels, predicted by Eq. (49) with $f = 2.0$, $\phi_m = 0.64$, and $\boldsymbol{a} = 0.5$ μm, at different values of the critical bending moment ($\boldsymbol{M}_c$). Arrow indicates the effect of increasing $\boldsymbol{M}_c$ for a given particle volume fraction.

4. Composite (or filled) suspensions and gels

Filler–matrix composite suspensions may be regarded as systems where rigid or viscoelastic particles (the filler), are embedded in a continuous viscoelastic material (the matrix) [68], as represented in Fig. 1g. In many cases, the matrix is a gel in itself, and the system is called a composite (or filled) gel. It has been found that the viscoelastic properties of composite suspensions/gels depend mainly on the rigidity of the matrix, the rigidity and volume fraction of the filler, and the interaction or affinity between the filler and the matrix [31]. If there is no interaction, this results in a decrease in the composite shear modulus with increasing volume fractions of the filler. If there is a strong interaction between both, this results in an increase in the shear modulus of the composite at increasing volume fractions of the filler if the latter is stiffer than the matrix [69], or the opposite trend if the filler is softer than the matrix. This is the behavior expected at small deformations. On the other hand, deviations from this behavior may occur under conditions of high strain due to slip at the matrix–filler interface, and or non-uniform distribution of stress and strain throughout the material [31,69,70].

The reinforcement effect of particles on the suspension/gel has been defined as the relative elastic modulus:

$$G_r^{'} = G_c^{'}/G_m^{'} \tag{50}$$

where $\boldsymbol{G}'_c$ is the elastic modulus of the composite suspension/gel, and $\boldsymbol{G}'_m$ is the elastic modulus of the matrix [31]. Smith [71] simplified the coefficients in Van der Poel's theoretical model [72] for calculating the shear modulus of a particulate composite. They considered an idealized composite material consisting of small spheres imbedded in a matrix. The spheres were of approximately the same size, firmly attached to the matrix, and uniformly distributed so that the composite material is macroscopically homogeneous and isotropic. The system was modeled as if each filler sphere (of radius a) was surrounded by a shell of matrix material (of radius $r = 1$), which in turn is embedded in the homogeneous material (Fig. 1h). The mechanical properties of this homogeneous material are assumed to be the same as the average macroscopic properties of the composite material (this

is somehow analogous to the effective medium approach). The final equation for G'_r can be reduced to:

$$\alpha\left(G'_r-1\right)^2+\beta\left(G'_r-1\right)+\delta=0 \tag{51}$$

where, for spherical particles:

$$\alpha=\left(8P-\phi^{7/3}S\right)[Q-3(M-1)\phi]-126P(M-1)\phi\left(1-\phi^{2/3}\right)^2 \tag{52}$$

$$\beta=17.5P[(3M+4.5)-3(M-1)\phi]-7.5\left(8P-5\phi^{7/3}\right)(M-1)\phi \tag{53}$$

$$\delta=-131.25P(M-1)\phi \tag{54}$$

and the quantities M, P, S, and Q depend on the elastic modulus of the filler particles, G'_f, and that of the matrix (G'_m), namely: $M=G'_f/G'_m$, $P=9.5M+8$, $S=76(M-1)$, and $Q=3M+4.5$.

Eq. (51) has two roots; the highest real root provides the correct value of G'_r. M is defined as the filler relative rigidity. The value of G'_f (and M) ranges from ∞ for perfectly rigid particles, to 0 for perfectly viscous particles. It has been noted [31] that while ϕ, ϕ_m, and G'_m can be determined by conducting experiments carefully, there does not appear to be a reliable experimental method for determination of G'_f.

Predictive curves of G'_r vs. ϕ for different values of M (0, 1, 10, and ∞) were obtained from Eqs. (51) to (54) (Fig. 15). It can be observed that when the rigidity of the filler is higher than that of the matrix ($G'_f > G'_m$), the filler produce a positive reinforcing effect on the suspension/gel; when $G'_f = G'_m$ the filler has no effect on G'_r, and when $G'_f < G'_m$ the filler has a negative effect. van Vliet [69] studied the rheological behavior of gels filled with emulsion droplets stabilized by different macromolecules, which were chosen to provide either no or a strong interaction between the filler and the matrix. For non-interacting particles, experimental data was close to the curve for $M=0$, which corresponds to the theoretical behavior of a spherical foam structure. He concluded that gels filled with non-interacting particles behave as if filled with particles with the rheological properties of water. For interacting particles, experimental data were both below and above the theoretical prediction for rigid particles ($M\to\infty$),

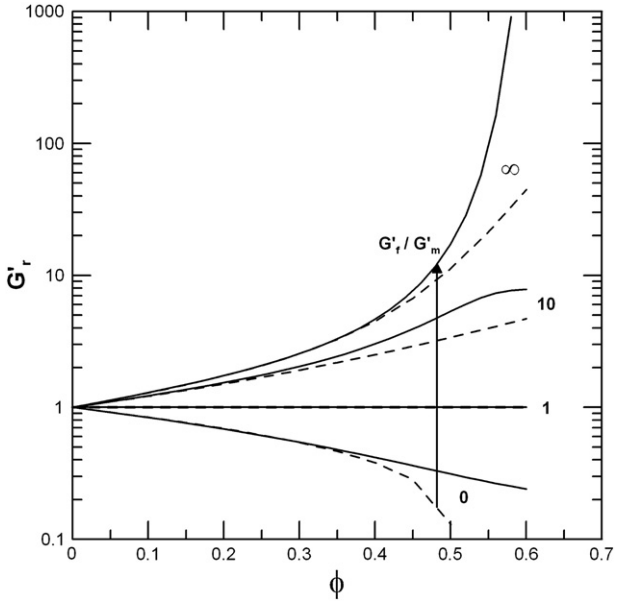

Fig. 15. Relative elastic modulus vs. particle volume fraction of composite gels, predicted by Eqs. (51) to (54) (dashed lines), and Eqs. (55) to (57) with $V=0.5$ and $\phi_m=0.64$ (solid lines), at different values of relative rigidity of the filler particles ($M=G'_f/G'_m$). Arrow indicates the effect of increasing M for a given particle volume fraction of particles.

depending on the type of gel matrix. The former result was attributed to either the emulsion droplets not being completely rigid, and/or the formation of an intermediate layer between the particles and the gel matrix with different rheological properties. The latter result was also reported by Kim et al. [73], and in both works it was attributed to particle aggregation (during matrix gelation), increasing their effective volume fraction. Another possibility is that Van der Poel–Smith's model (Eqs. (51) to (54)) simply underestimates experimental values of G'_r.

One of the approximate solutions of Van der Poel–Smith's model is the well known Kerner's equation [74], which predicts G'_r values even lower than Van der Poel–Smith's model, significantly when the volume fraction of filler exceeds 0.2 [71]. Lewis and Nielsen [75] modified Kerner's equation introducing a term that accounts for the maximum volume fraction of the filler:

$$G'_r=\frac{1+A\cdot B\cdot\phi}{1-B\cdot\left[1-\exp\left(-\frac{\phi}{1-\phi/\phi_m}\right)\right]} \tag{55}$$

$$A=\frac{7-5\cdot V}{8-10\cdot V} \tag{56}$$

$$B=\frac{M-1}{M+A} \tag{57}$$

where V is the particles Poisson's ratio (for spheres $V=0.5$, then $A=1.5$) [31]. Using values of $V=0.5$ and $\phi_m\approx0.64$ in Eqs. (55) to (57) [70], predictive curves of G'_r vs. ϕ for different values of M (0, 1, 10, and ∞) were obtained (Fig. 15). It can be observed that Kerner–Lewis and Nielsen's model predicts G'_r values higher than Van der Poel–Smith's model, significantly at volume fractions higher than about 0.3. Brownsey et al. [70] studied the rheological behavior of composite gels consisting of spherical deformable filler particles embedded in a gelatin gel matrix. They found that Kerner–Lewis and Nielsen's model predicted lower values of reinforcement compared to experimental data, but still in reasonable agreement. They attributed this difference to a lower real value of the maximum packing fraction of the composite, compared to the theoretical value of 0.64. Carnali and Zhou [76] studied the rheological behavior of starch gels, considering them as composites where the dispersed starch granules (the fillers) have a reinforcing effect on the amylose gel (the matrix). They fitted experimental data with the Kerner–Lewis and Nielsen's model, and obtained highly satisfactory agreement at $\phi_m=0.72$, $M=12$ for systems gelatinized at 70 °C, and $\phi_m=0.74$, $M=8$ for systems gelatinized at 85 °C.

Analogously to Eq. (50), the relative complex modulus may be defined as:

$$G^*_r=G^*_c/G^*_m \tag{58}$$

where G^*_c and G^*_m are the complex shear moduli of the composite suspension/gel and the matrix, respectively. Pal [68] used the self-consistent or effective medium approach to derive an expression for the relative complex modulus of composite suspensions/gels with solid viscoelastic particles ($G^*_f >> G^*_m$):

$$G^*_r=\left(\frac{G^*_r-G^*_f/G^*_m}{1-G^*_f/G^*_m}\right)^{2.5}\cdot\left(1-\frac{\phi}{\phi_m}\right)^{-2.5\cdot\phi_m} \tag{59}$$

where G^*_f is the complex modulus of the filler particles. Eq. (59) is analogous to Krieger and Dougherty's equation (Eq. (3)). For composite gels filled with rigid particles, $G^*_f\to\infty$ and the first term of the product is reduced to one. For this type of composites, Pal [68] and Manski et al. [77] fitted G^*_r vs. ϕ experimental data with Eq. (59) and obtained good predictions with ϕ_m values of 0.5 and 0.6, respectively. Using a value of $\phi_m\approx0.6$ in Eq. (59), predictive curves of G^*_r vs. ϕ were obtained at different values of G^*_f/G^*_m (10, 100, and ∞) (Fig. 16). It can be observed that for a given volume fraction of the filler, the relative complex

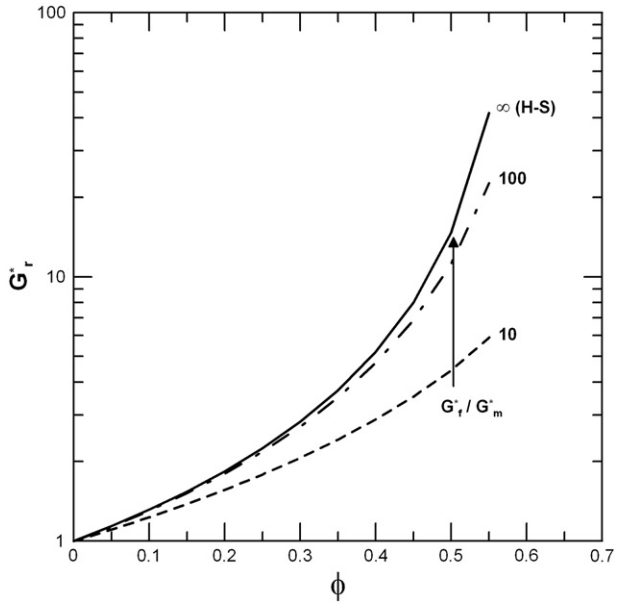

Fig. 16. Relative complex modulus vs. particle volume fraction of composite gels, predicted by Eq. (59) with $\phi_m = 0.6$, at different values of relative complex modulus of the filler particles (G^*_f/G^*_m). Arrow indicates the effect of increasing G^*_f/G^*_m for a given particle volume fraction.

modulus of the composite increases at increasing values of the relative complex modulus of the filler.

5. Conclusions

From the many models proposed in the literature to describe the shear viscosity of flowing suspensions, the Krieger–Dougherty equation was selected because of its effectiveness, simplicity, and versatility. The original expression (Eq. (4)) is well known to effectively predict the relative viscosity of hard-sphere suspensions. The many deviations from this ideal case may be accounted by simple modifications of the original equation, either by replacing the particle volume fraction by an effective volume fraction, or by replacing the maximum packing fraction by an effective maximum packing fraction. Theoretical expressions and empirical values have been reported for both the effective volume fraction and the effective maximum packing fraction of each type of suspension, and used in this work to reproduce predictive curves of relative viscosity vs. particle volume fraction within typical ranges of experimental data.

In the case of aggregated suspensions, they form gels above the percolation concentration, showing solid-like viscoelasticity. Several theoretical models for the yield stress and elastic modulus of these gels have been reported in the literature. We demonstrated the analogy between these models, and used typical empirical values to plot predictive curves of yield stress and elastic modulus vs. particle volume fraction within practical ranges of experimental data. The same was done for the relative elastic and relative complex moduli of filler–matrix composite gels.

Acknowledgments

Author D.B.G. gratefully acknowledges financial support from CONICET Argentina.

References

[1] Sennet P, Olivier JP. In: Gushee DE, editor. Chemistry and physics of interfaces. American Society Publications; 1965. Chapter 7.
[2] Brader JM. J Phys Condens Matter 2010:363101.
[3] Barnes HA. A handbook of elementary rheology, the University of Wales Institute of Non-Newtonian Fluid Mechanics; 2000. Chapter 15.
[4] Zhou Z, Scales PJ, Boger DV. Chem Eng Sci 2001;56:2901.
[5] Qin K, Zaman AA. J Colloid Interface Sci 2003;266:461.
[6] Russel WB. J Rheol 1980;24:287.
[7] Tadros ThF. Adv Colloid Interface Sci 1996;68:97.
[8] Russel WB, Sperry PR. Prog Org Coat 1994;23:305.
[9] Metzner AB. J Rheol 1985;29:739.
[10] Russel WB, Saville DA, Schowalter WR. In: Batchelor GK, editor. Colloidal dispersions. Cambridge University Press; 1989. Chapter 14.
[11] Einstein A. Ann Phys 1906;19:289.
[12] Einstein A. Ann Phys 1911;34:591.
[13] Krieger IM, Dougherty TJ. Trans Soc Rheol 1959;3:137.
[14] Quemada D, Berli C. Adv Colloid Interface Sci 2002;98:51.
[15] Servais C, Jones R, Roberts I. J Food Eng 2002;51:201.
[16] Pusey PN, van Megen W. Nature 1986;320:340.
[17] Loveday SM, Creamer LK, Singh H, Rao MA. J Food Sci 2007;72:R101.
[18] Pham KN, Puertas AM, Bergenholtz J, Egelhaaf SU, Moussaïd A, Pusey PN, et al. Science 2002;296:5565.
[19] Eckert T, Bartsch E. J Phys Condens Matter 2004;16:S4937.
[20] Sztucki M, Narayanan T, Belina G, Moussaïd A. Phys Rev E 2006;74 051504-1.
[21] Laurati M, Petekidis G, Koumakis N, Cardinaux F, Schofield AB, Brader JM, et al. J Chem Phys 2009;130 134907-1.
[22] Gates ME, Fuchs M, Kroy K, Poon WCK, Puertas AM. J Phys Condens Matter 2004;16:S4861.
[23] Brader JM, Cates ME, Fuchs M. Phys Rev Lett 2008;101 138301-1.
[24] Di Cola E, Moussad A, Sztucki M, Narayanan T, Zaccarelli E. J Chem Phys 2009;131 144903-1.
[25] Brader JM, Siebenbürger M, Ballauff M, Reinheimer K, Wilhelm M, Frey SJ, et al. Phys Rev E 2010;82 061401-1.
[26] Mewis J, Wagner NJ. J Non-Newtonian Fluid Mech 2009;157:147.
[27] Genovese DB, Lozano JE, Rao MA. J Food Sci 2007;72:R11.
[28] Brady JF. Chem Eng Sci 2001;56:2921.
[29] Phung TN, Brady JF, Bossis G. J Fluid Mech 1996;313:181.
[30] Pan W, Caswell B, Karniadakis GE. Langmuir 2010;26:133.
[31] Rao MA. In: Barbosa-Cánovas GV, editor. Rheology of fluid and semisolid foods. Springer; 2007. Chapters 2 and 6.
[32] Barnes HA. J Rheol 1989;33:329.
[33] Potanin AA. J Colloid Interface Sci 1993;156:143.
[34] Chen H, Ding Y, Tan C. New J Phys 2007;9 367-1.
[35] Iwashita T, Yamamoto R. Phys Rev E 2009;80 061402-1.
[36] Simha R. J Phys Chem 1940;44:25.
[37] Kitano T, Kataoka T, Shirota T. Rheol Acta 1981;20:207.
[38] Funk JE, Dinger DR. Predictive process control of crowded particulate suspensions. Springer; 1993. Chapter 5.
[39] Farris RJ. Trans Soc Rheol 1968;12:281.
[40] Snabre P, Mills P. J Phys III 1996;6:1835.
[41] McClements DJ. In: Clydesdale FM, editor. Food emulsions. CRC Press; 1999. Chapter 3.
[42] Everett DH. Pure Appl Chem 1972;31:577.
[43] Brady JF, Vicic M. J Rheol 1995;39:545.
[44] Berli CLA, Deiber JA, Añón MC. Food Hydrocolloids 1999;13:507.
[45] Snabre P, Mills P. J Phys III 1996;6:1811.
[46] Lapasin R, Grassi M, Pricl S. Chem Eng J 1996;64:99.
[47] Coussot P, Ancey C. Phys Rev E 1999;59:4445.
[48] Ogawa A, Yamada H, Matsuda S, Okajima K. J Rheol 1997;41:769.
[49] Hidalgo-Álvarez R, Martín A, Fernández A, Bastos D, Martínez F, de las Nieves FJ. Adv Colloid Interface Sci 1996;67:1.
[50] Rubio-Hernández FJ, Carrique F, Ruiz-Reina E. Adv Colloid Interface Sci 2004;107:51.
[51] Luckham PF, Rossi SR. Adv Colloid Interface Sci 1999;82:43.
[52] Buscall R. J Chem Soc Faraday Trans 1991;87:1365.
[53] Buscall R. Colloids Surf A 1994;83:33.
[54] Phan S-E, Russel WB, Cheng Z, Zhu J, Chaikin PM, Dunsmuir JH, et al. Phys Rev E 1996;54:6633.
[55] Potanin AA, De Rooij R, Van den Ende D, Mellema J. J Chem Phys 1995;102:5845.
[56] Goodwin JW, Reynolds PA. Curr Opin Colloid Interface Sci 1998;3:401.
[57] Channell GM, Zukoski CF. AIChE J 1997;43:1700.
[58] Dickinson E. J Colloid Interface Sci 2000;225:2.
[59] Uriev NB, Ladyzhinsky IY. Colloids Surf A 1996;108:1.
[60] Chougnet A, Palermo T, Audibert A, Moan M. Cem Concr Res 2008;38:1297.
[61] Pantina JP, Furst EM. Langmuir 2006;22:5282.
[62] Wessel R, Ball C. Phys Rev A 1992;46:R3008.
[63] Collins IR. J Colloid Interface Sci 1992;178:361.
[64] Tadros T. Adv Colloid Interface Sci 2004;108–109:227.
[65] Potanin AA, Russel WB. Phys Rev E 1996;53:3702.
[66] Shih W-H, Shih WY, Kim S-I, Liu J, Aksay IA. Phys Rev A 1990;42:4772.
[67] Furst EM, Pantina JP. Phys Rev E 2007;75:050402-1.
[68] Pal R. J Colloid Interface Sci 2002;245:171.
[69] van Vliet T. Colloid Polym Sci 1988;266:518.
[70] Brownsey GJ, Ellis HS, Ridout MJ, Ring SG. J Rheol 1987;31:635.
[71] Smith JC. J Res Natl Bur Stand 1975;79A:419.
[72] van der Poel C. Rheol Acta 1958;1:198.
[73] Kim K-H, Renkema JMS, van Vliet T. Food Hydrocolloids 2001;15:295.
[74] Kerner EH. Proc Phys Soc Sect B 1956;69:808.
[75] Lewis TB, Nielsen LE. J Appl Polym Sci 1970;14:1449.
[76] Carnali JO, Zhou Y. J Rheol 1996;40:221.
[77] Manski JM, Kretzer IMJ, van Brenk S, van der Goot AJ, Boom RM. Food Hydrocolloids 2007;21:73.